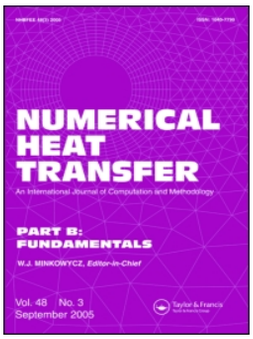

Taylor & Francis
Taylor & Francis Group

Numerical Heat Transfer, Part B: Fundamentals
An International Journal of Computation and Methodology

ISSN: 1040-7790 (Print) 1521-0626 (Online) Journal homepage: www.tandfonline.com/journals/unhb20

General fully implicit discretization of the diffusion term for the finite volume method

M. Darwish, L. Mangani & F. Moukalled

To cite this article: M. Darwish, L. Mangani & F. Moukalled (2017) General fully implicit discretization of the diffusion term for the finite volume method, Numerical Heat Transfer, Part B: Fundamentals, 71:6, 506-532, DOI: 10.1080/10407790.2017.1330060

To link to this article: https://doi.org/10.1080/10407790.2017.1330060

NUMERICAL HEAT TRANSFER, PART B
2017, VOL. 71, NO. 6, 506–532
https://doi.org/10.1080/10407790.2017.1330060

Taylor & Francis
Taylor & Francis Group

General fully implicit discretization of the diffusion term for the finite volume method

M. Darwish[a], L. Mangani[b], and F. Moukalled[a]

[a]Department of Mechanical Engineering, American University of Beirut, Beirut, Lebanon; [b]Hochschule Luzern, Technik und Architektur, Horw, Switzerland

ABSTRACT

In this paper, a fully implicit method for the discretization of the diffusion term is presented in the context of the cell-centered finite volume method. The newly developed fully implicit method is denoted by the modified implicit nonlinear diffusion (MIND) scheme. The method is used to solve several isotropic and anisotropic diffusion problems in two-dimensional domains covered with structured (quadrilateral elements) and unstructured (triangular elements) grid systems. The comparison of generated results with similar ones obtained using the semi-implicit scheme demonstrates the superior robustness and accuracy of the MIND scheme and its good convergence characteristics for all types of meshes.

ARTICLE HISTORY
Received 5 January 2017
Accepted 27 April 2017

Introduction

The cell-centered finite volume method (FVM) is one of the most popular numerical techniques in computational fluid dynamics (CFD) [1–3]. In fact, the leading commercial CFD packages [4–6] and the majority of open source CFD codes [7, 8] use the FVM for the discretization of their equations. This popularity is due to several properties, which include conservativeness (i.e., conservation of quantities is enforced for coarse and fine meshes alike), the ability to define biased discretization profiles (very useful for the treatment of convection), and the capacity to work with two- and three-dimensional elements of any polygonal shape without the need for shape functions [9].

Despite these desirable attributes, the widely adopted approach for the discretization of the diffusion term in the FVM, denoted here by the semi-implicit (SI) approach [10–18], breaks down in terms of implicitness on nonorthogonal meshes and/or for anisotropic diffusion coefficients. This is due to the discretization approach followed in the semi-implicit method, wherein the diffusion flux is split into an implicit (aligned, orthogonal) and an explicit (nonorthogonal, cross-diffusion) component. In the resulting discretized system of equations, the implicit part is added to the coefficient matrix on the left-hand side, while the explicit part is added to the source vector on the right-hand side. This approach allows for an accurate resolution of the diffusion term at the cost of an increase in the number of iterations to convergence and in certain cases to oscillations or divergence in the solution process.

Even though several fully implicit schemes for the discretization of the anisotropic diffusion term in the context of the FVM have been developed [19–23], the fully implicit approach is still not popular within the CFD community. This is due to the complexities associated with its implementation, especially in unstructured grid systems, and because many of the developed techniques fail to enforce the discrete maximum/minimum principle (DMP) [24–26], thereby not justifying the added

CONTACT F. Moukalled memouk@aub.edu.lb; fmukalled@aub.edu.lb Department of Mechanical Engineering, American University of Beirut, P.O. Box 11-0236, Riad El Solh, Beirut 1107 2020, Lebanon.
Color versions of one or more of the figures in this article can be found online at www.tandfonline.com/unhb.

Nomenclature

C	main grid point at an element centroid
$\boldsymbol{d}_{CF}$	vector joining the two points C and F
d_{CF}	magnitude of $\boldsymbol{d}_{CF}$
$\boldsymbol{e}_{CF}$	unit vector in the direction of $\boldsymbol{d}_{CF}$
$\boldsymbol{E}, \boldsymbol{E}', \tilde{\boldsymbol{E}}'$	distance vectors in the direction of $\boldsymbol{d}_{CF}$
$E, E', \tilde{E}'$	magnitude of $\boldsymbol{E}$, $\boldsymbol{E}'$, and $\tilde{\boldsymbol{E}}'$, respectively
F	neighbor of element C
f	face
J	diffusion flux
$\boldsymbol{K}$	diffusion coefficient tensor
k_{xx}, k_{xy}	diffusion coefficients
N_C, N_F	location used in the calculation of the non-orthogonal part of J_C and J_F, respectively
Q	source term in conservation equation
$\boldsymbol{S}, \boldsymbol{S}', \tilde{\boldsymbol{S}}'$	surface and modified surface vectors
$S, S', \tilde{S}'$	magnitude of $\boldsymbol{S}, \boldsymbol{S}'$, and $\tilde{\boldsymbol{S}}'$
$\boldsymbol{n}', \boldsymbol{t}$	unit vector in the direction of $\boldsymbol{S}'$ and $\boldsymbol{T}$, respectively
$\boldsymbol{T}, \boldsymbol{T}', \tilde{\boldsymbol{T}}'$	vectors equal to $\boldsymbol{S}-\boldsymbol{E}$, $\boldsymbol{S}'-\boldsymbol{E}'$, and $\tilde{\boldsymbol{S}}'-\tilde{\boldsymbol{E}}'$, respectively
V	cell volume

Greek symbols

ϕ	general variable
δ_C, δ_F	averaging factors
$\delta_C^{\bullet}$, $\delta_F^{\bullet}$	averaging factors satisfying Eq. (13)
θ	rotation angle

Subscripts

b	refers to boundary
C	refers to main grid point
f	refers to element face
F	refers to the F grid point
∞	refers to free stream value

Superscripts

T	refers to the transpose of a vector
$\bar{}$	refers to an interpolated value

intricacies. The DMP states that no new minima or maxima should arise in the solution of simple elliptic or parabolic problems. This property is crucial to numerical schemes in certain applications where, for example, negative values are simply not physical. A somewhat similar constraint applies to the treatment of the convection term denoted by the convection boundedness criterion [27, 28].

As mentioned above, numerous studies related to the discretization of the anisotropic diffusion term have appeared in the literature. Liu et al. [29] reported on two finite volume-based methods for the discretization of the diffusion term designated by the direct (a 13-point scheme) and the balance-point (a nine-point scheme) methods. Umansky et al. [30] discussed the construction of a finite-difference scheme for a strongly anisotropic diffusion equation on a misaligned grid and performed a quantitative assessment of the numerical error for several test cases. Truscott and Turner [31] investigated the accuracy of the control-volume finite-element method for simulating strongly anisotropic diffusion problems and demonstrated that the use of a Gauss–Green gradient reconstruction technique greatly improves the accuracy of predictions over the classical finite-element shape function technique. Aavatsmark [32] and Aavatsmark et al. [33] developed a consistent finite-volume flux approximation in heterogeneous media with discontinuous piecewise constant anisotropic diffusion tensors. Manzini and Putti [34] discussed the mesh-locking issue encountered in solving anisotropic diffusion problems. Moreover, the diffusion schemes developed in [35–39] satisfy the monotonicity condition, which is a simplified version of the DMP ensuring positivity of the solution. On the other hand, diffusion schemes satisfying the DMP are scarce and include the ones reported in [40, 41].

In this paper, a modification to the nonlinear two-flux diffusion method of Lipnikov et al. [42] is designed and generalized to yield a fully implicit diffusion scheme that is simpler to implement and with lower overhead. While the Lipnikov et al. scheme [42] satisfies only the monotonicity condition by guaranteeing solution non-negativity, results obtained for all problems considered in this work indicate that the newly developed discretization scheme satisfies the DMP. It is worth noting that DMP-preserving schemes apply to a special set of variables that are not allowed to change sign. This requirement is not as restrictive as it appears since absolute temperature and pressure, turbulence kinetic energy, turbulent eddy dissipation, turbulence eddy frequency, mass fractions of species, and volume fractions for example all do satisfy this condition.

In what follows, the diffusion equation is first presented followed by a review of the widely adopted semi-implicit discretization scheme. Then the two-flux nonlinear diffusion discretization scheme of Lipnikov et al. [42] is explained using a more approachable notation than in the original paper, setting

the ground for presenting the modified implicit nonlinear diffusion (MIND) scheme. Finally several test problems are solved to evaluate the performance and accuracy of the MIND scheme for several mesh sizes.

Governing equation

The diffusion equation considered in this work can be written as

$$\underbrace{-\nabla\cdot(\boldsymbol{K}\nabla\phi)}_{\text{Diffusion term}} = \underbrace{Q}_{\text{Source term}} \tag{1}$$

where ϕ, $\boldsymbol{K}$, and Q represent the dependent variable, the diffusion coefficient tensor, and the source term, respectively. Equation (1) is solved numerically over a domain D of boundary ∂D and subject to one or more boundary conditions of the Dirichlet, von Neumann, Robin, or symmetry type. The discretization procedure follows the FVM [1–3, 9] in which the domain is subdivided into several nonoverlapping elements. The source term is evaluated by assuming the value of the dependent variable at the element centroid to represent the average value over the element volume. The discretization of the diffusion term, the subject of this article, is detailed in the following sections.

Semi-Implicit discretization scheme

In this section, a brief review of the semi-implicit treatment for the discretization of the diffusion operator with anisotropic coefficients is presented; for additional details the reader is referred to references [13–18]. Considering an anisotropic diffusion problem with no discontinuity in the heterogeneous coefficient tensor $\boldsymbol{K}$, the discretization is performed by first reformulating the operation order as follows [10] (Figure 1*a*):

$$-\boldsymbol{K}_f\overline{\nabla\phi_f}\cdot\boldsymbol{S}_f = -\overline{\nabla\phi_f}\cdot\left[\boldsymbol{K}_f\right]^T\boldsymbol{S}_f = -\overline{\nabla\phi_f}\cdot\boldsymbol{S}'_f \tag{2}$$

where $\boldsymbol{S}_f$ is the surface vector and $\boldsymbol{S}'_f$ is a modified surface vector.

Then the discretization proceeds by linearizing the diffusion term along the component of $\boldsymbol{S}'_f$ aligned with the CF direction and treating the remainder explicitly, leading to

$$\begin{aligned}\overline{\nabla\phi_f}\cdot\boldsymbol{S}'_f &= \overline{\nabla\phi_f}\cdot\boldsymbol{E}'_f + \overline{\nabla\phi_f}\cdot\left(\boldsymbol{S}'_f-\boldsymbol{E}'_f\right) = \underbrace{\frac{(\phi_F-\phi_C)}{d_{CF}}E'_f}_{\text{implicit}}\\ &+\underbrace{\overline{\nabla\phi_f}\cdot\boldsymbol{T}'_f}_{\text{explicit}} = \frac{E'_f}{d_{CF}}\phi_F - \frac{E'_f}{d_{CF}}\phi_C + \overline{\nabla\phi_f}\cdot\boldsymbol{T}'_f\end{aligned} \tag{3}$$

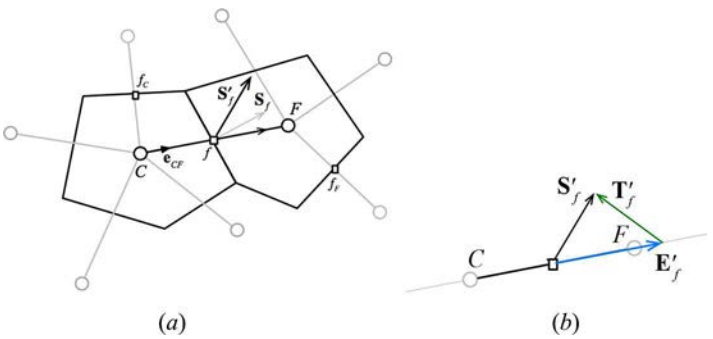

Figure 1. (*a*) The surface vector $\boldsymbol{S}_f$ and the modified surface vector $\boldsymbol{S}'_f$; (*b*) Decomposing the nonorthogonal diffusion component using the largest linearization vector.

The vector $\boldsymbol{S}_f'$ can be decomposed in several ways [13]. However, as reported by Demirdzic [13], the optimal approach is to maximize the linearized term (Figure 1*b*) with $\boldsymbol{E}_f'$ and $\boldsymbol{T}_f'$ computed as

$$\boldsymbol{E}_f' = \frac{S_f'}{\boldsymbol{n}_f' \cdot \boldsymbol{e}_{\mathrm{CF}}} \boldsymbol{e}_{\mathrm{CF}} \quad \boldsymbol{T}_f' = \boldsymbol{S}_f' - \frac{S_f'}{\boldsymbol{n}_f' \cdot \boldsymbol{e}_{\mathrm{CF}}} \boldsymbol{e}_{\mathrm{CF}} = S_f' \left(\boldsymbol{n}_f' - \frac{\boldsymbol{e}_{\mathrm{CF}}}{\boldsymbol{n}_f' \cdot \boldsymbol{e}_{\mathrm{CF}}} \right) = T_f' \boldsymbol{t}_f' \tag{4}$$

where $\boldsymbol{n}_f', \boldsymbol{e}_{\mathrm{CF}}$, and $\boldsymbol{t}_f'$ are unit vectors in the direction of $\boldsymbol{S}_f'$, CF, and $\boldsymbol{T}_f'$, respectively.

Nonlinear two-flux approximation scheme

The nonlinear two-flux approximation scheme was originally formulated by Le Potier [43] to allow for a consistent resolution of diffusion transport in porous media. The scheme was further developed [40] to ensure satisfaction of the minimum/maximum principle for low-quality meshes and/or highly anisotropic diffusion. The nonlinear two-flux discretization scheme presented in this paper is based on the scheme of Lipnikov et al. [42]. In Lipnikov's method, the diffusion flux is computed using a directional gradient discretization for the nonorthogonal part. As illustrated in Figure 2, the diffusion flux at face f (Figure 2*a*) can be computed in two different ways using a directional gradient defined either in terms of C and N_{C} (Figure 2*b*) or in terms of F and N_F (Figure 2*c*). The resulting two expressions for the diffusion flux are given by

$$J_{\mathrm{C}} = \overline{\nabla \phi_f} \cdot \boldsymbol{S}_f' = \overline{\nabla \phi_f} \cdot \left(\boldsymbol{E}_f' + \boldsymbol{T}_f' \right) = \frac{E_f'}{d_{\mathrm{CF}}} (\phi_{\mathrm{F}} - \phi_{\mathrm{C}}) + \frac{T_f'}{d_{\mathrm{CN_C}}} \left(\phi_{\mathrm{N_C}} - \phi_{\mathrm{C}} \right) \tag{5}$$

$$J_{\mathrm{F}} = \overline{\nabla \phi_f} \cdot \tilde{\boldsymbol{S}}_f' = \overline{\nabla \phi_f} \cdot \left(\tilde{\boldsymbol{E}}_f' + \tilde{\boldsymbol{T}}_f' \right) = \frac{\tilde{E}_f'}{d_{\mathrm{CF}}} (\phi_{\mathrm{C}} - \phi_{\mathrm{F}}) + \frac{\tilde{T}_f'}{d_{\mathrm{FN_F}}} \left(\phi_{\mathrm{N_F}} - \phi_{\mathrm{F}} \right) \tag{6}$$

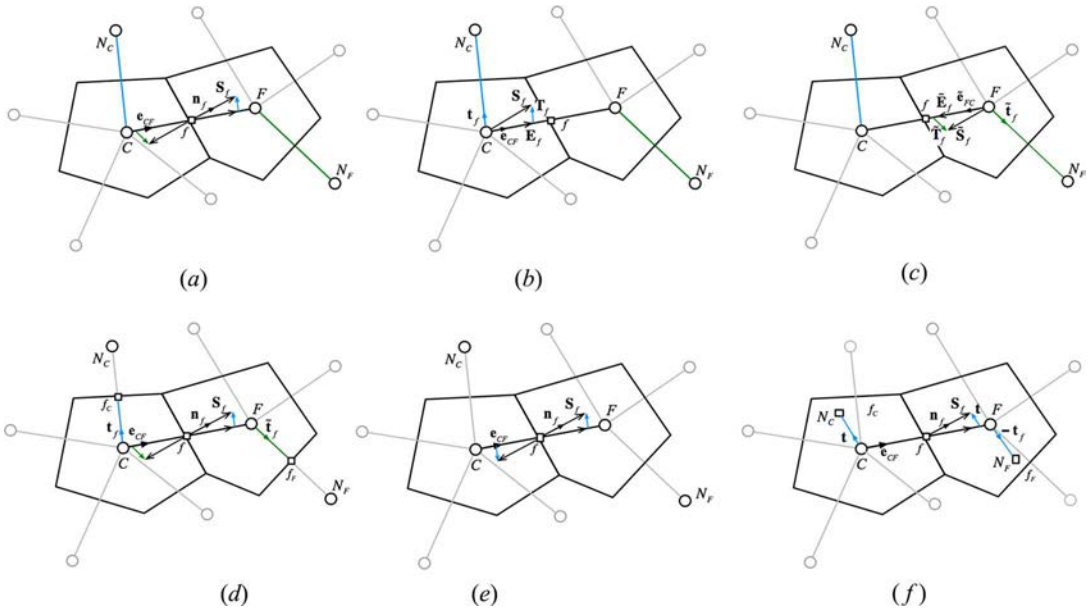

Figure 2. (*a*) The nonorthogonal gradient stencil; (*b*) the nonorthogonal gradient stencil resolved from the owner cell *C*; (*c*) the nonorthogonal gradient stencil resolved from the neighbor cell *F*; (*d*) the nonlinear diffusion stencil; (*e*) the semi-implicit discretization; and (*f*) the modified nonlinear diffusion stencil.

It should be noted that the surface vector used in the calculation of the flux J_F is opposite to that used in the calculation of J_C, i.e.,

$$\tilde{\boldsymbol{S}}'_f = -\boldsymbol{S}'_f \tag{7}$$

Using the above two expressions, the flux at the centroid f of the face in the two flux approximation scheme is computed as

$$\begin{aligned}\overline{\nabla\phi_f}\cdot\boldsymbol{S}'_f = \delta_C J_C - \delta_F J_F = \delta_C\left[\frac{E'_f}{d_{CF}}(\phi_F-\phi_C)+\frac{T'_f}{d_{CN_C}}(\phi_{N_C}-\phi_C)\right]\\ -\delta_F\left[\frac{\tilde{E}'_f}{d_{CF}}(\phi_C-\phi_F)+\frac{\tilde{T}'_f}{d_{FN_F}}(\phi_{N_F}-\phi_F)\right]\end{aligned} \tag{8}$$

where δ_C and δ_F are averaging factors to be defined but that sum to 1, and $\boldsymbol{S}'_f$ and $\tilde{\boldsymbol{S}}'_f$ are the equivalent surface vectors decomposed into

$$\boldsymbol{S}'_f = \boldsymbol{E}'_f + \boldsymbol{T}'_f \quad \tilde{\boldsymbol{S}}'_f = \tilde{\boldsymbol{E}}'_f + \tilde{\boldsymbol{T}}'_f \tag{9}$$

Equation (8) can be rearranged and rewritten as

$$\begin{aligned}\overline{\nabla\phi_f}\cdot\boldsymbol{S}'_f = &\left[\delta_C\frac{E'_f}{d_{CF}}+\delta_F\left(\frac{\tilde{E}'_f}{d_{CF}}+\frac{\tilde{T}'_f}{d_{FN_F}}\right)\right]\phi_F\\ &-\left[\delta_F\frac{\tilde{E}'_f}{d_{CF}}+\delta_C\left(\frac{E'_f}{d_{CF}}+\frac{T'_f}{d_{CN_C}}\right)\right]\phi_C+\delta_C\frac{T'_f}{d_{CN_C}}\phi_{N_C}-\delta_F\frac{\tilde{T}'_f}{d_{FN_F}}\phi_{N_F}\end{aligned} \tag{10}$$

Note that generally

$$\tilde{\boldsymbol{E}}'_f \neq -\boldsymbol{E}'_f \quad \tilde{\boldsymbol{T}}'_f \neq -\boldsymbol{T}'_f \tag{11}$$

At this point arithmetic averaging can be used with the factors δ_C and δ_F set to 0.5, or defined in terms of the mesh geometry as

$$\delta_C = \frac{d_{fF}}{d_{Cf}+d_{fF}} \quad \delta_F = \frac{d_{Cf}}{d_{Cf}+d_{fF}} \tag{12}$$

In this case, the terms involving ϕ_{N_C} and ϕ_{N_F} are treated explicitly.

In the work of Lipnikov et al. [42], these two terms are eliminated using a special averaging that satisfies the relations

$$\delta_C+\delta_F = 1 \quad \delta_C\frac{T'_f}{d_{CN_C}}\phi_{N_C}-\delta_F\frac{\tilde{T}'_f}{d_{FN_F}}\phi_{N_F}=0 \tag{13}$$

With the neighboring values simplified, the diffusion expression becomes fully implicit and can be written as

$$\overline{\nabla\phi_f}\cdot\boldsymbol{S}'_f = \left[\delta^\bullet_C\frac{E'_f}{d_{CF}}+\delta^\bullet_F\left(\frac{\tilde{E}'_f}{d_{CF}}+\frac{\tilde{T}'_f}{d_{FN_F}}\right)\right]\phi_F-\left[\delta^\bullet_F\frac{\tilde{E}'_f}{d_{CF}}+\delta^\bullet_C\left(\frac{E'_f}{d_{CF}}+\frac{T'_f}{d_{CN_C}}\right)\right]\phi_C \tag{14}$$

where now $\delta^\bullet_C$ and $\delta^\bullet_F$ are solutions to Eq. (13).

Computing T' and $\tilde{T}'$

In Eq. (13), $\boldsymbol{T}'$ (and $\tilde{\boldsymbol{T}}'$) is first computed by looping over the neighbors of C (and F) and selecting the neighbor N_C for C (and N_F for F) that satisfies the following two conditions:

1. The dot product $\boldsymbol{e}_{CN_C} \cdot \boldsymbol{n}'$ (and $\boldsymbol{e}_{FN_F} \cdot \tilde{\boldsymbol{n}}'$) should be the smallest possible, i.e., $\boldsymbol{d}_{CN_C}$ should be the closest to being normal to $\boldsymbol{S}'$ (the same is true for $\boldsymbol{d}_{FN_F}$ and $\tilde{\boldsymbol{S}}'$).
2. Since $\boldsymbol{S}' = -\tilde{\boldsymbol{S}}'$, the dot products $\boldsymbol{e}_{FN_F} \cdot \tilde{\boldsymbol{n}}'$ and $\boldsymbol{d}_{CN_C} \cdot \boldsymbol{d}_{FN_F}$ should be negative.

These requirements ensure that the selected points will be the farthest apart, thus allowing for better approximation of the cross gradient.

Modified implicit nonlinear diffusion scheme

In the Lipnikov method, the search procedure is time-consuming and while for isotropic coefficients the search can be performed once and its results stored for later use, in the case of anisotropic coefficients the search has to be performed for each variable. Furthermore, for solution-dependent anisotropic coefficients the search has to be repeated, at the end of any iteration, for each of the relevant variables. In addition for many element configurations, especially for tetragonal, prismatic, and pyramidal elements the selected neighbors can still be at undesirable locations. As shown in Figure 2(*d*), with the nonlinear two-flux approximation scheme the directions of $\boldsymbol{T}'_f$ and $\tilde{\boldsymbol{T}}'_f$ are respectively defined by the directions of the lines connecting the centroids of cells C and F with the selected neighboring element centroids N_C and N_F. This can result in $\boldsymbol{T}'_f$ and $\tilde{\boldsymbol{T}}'_f$ having very different values, which can be detrimental to the quality of the cross-diffusion term especially in three-dimensional calculations where the two vectors do not lie necessarily in the same plane. In a semi-implicit discretization (Figure 2*e*), the direction of the nonorthogonal component would be governed by the relation between $\boldsymbol{S}'_f$ and $\boldsymbol{d}_f$.

Work on addressing these issues resulted in the MIND scheme, which shares many of the characteristics of the Lipnikov et al. scheme [42], while addressing some of its shortcomings. In the MIND method, the cross nodes N_C and N_F are constructed as virtual points in a similar way as with high-resolution convection schemes [44–46] on unstructured grids [47]. This results in a method that does not require a neighbor search, is simple to implement, and allows for a straightforward handling of inter-block interfaces [48, 49].

It should be noted that the MIND scheme proposed in the present work does not account for piecewise-constant discontinuous tensors in a consistent way. The method may be extended by reconstructing gradient from harmonic averaging points [50], which may necessitate reconstructing the gradient for each component independently. This is currently under consideration.

With MIND, the nodes N_C and N_F shown in Figure 2(*f*) are reconstructed and the ϕ_{N_C} and ϕ_{N_F} values are computed using the gradients at C and F, respectively, as

$$\phi_{N_C} = \phi_C + \nabla\phi_C \cdot \boldsymbol{d}_{CN_C} \quad \phi_{N_F} = \phi_F + \nabla\phi_F \cdot \boldsymbol{d}_{FN_F} \tag{15}$$

The vectors $\boldsymbol{d}_{CN_C}$ and $\boldsymbol{d}_{FN_F}$ define the directions of $\boldsymbol{T}'_f$ and $\tilde{\boldsymbol{T}}'_f$, respectively, with their magnitudes related to length scales of the elements. Thus the virtual cross-diffusion points can be defined such that $\boldsymbol{T}'_f$ and $\tilde{\boldsymbol{T}}'_f$ have equal magnitudes but opposite directions, i.e., the virtual nodes are constructed such that

$$\boldsymbol{S}'_f = \boldsymbol{E}'_f + \boldsymbol{T}'_f = -\tilde{\boldsymbol{S}}'_f \quad \boldsymbol{E}'_f = -\tilde{\boldsymbol{E}}'_f \quad \boldsymbol{T}'_f = -\tilde{\boldsymbol{T}}'_f \tag{16}$$

leading to the following discretized diffusion flux:

$$\begin{aligned}\overline{\nabla\phi_f} \cdot \boldsymbol{S}'_f &= \overline{\nabla\phi_f} \cdot \boldsymbol{E}'_f + \overline{\nabla\phi_f} \cdot \boldsymbol{T}'_f = \frac{(\phi_F - \phi_C)}{d_{CF}} E'_f + \delta_C \nabla\phi_C \cdot \boldsymbol{T}'_f + \delta_F \nabla\phi_F \cdot \boldsymbol{T}'_f \\ &= \left(\frac{E'_f}{d_{CF}} + \delta_F \frac{T'_f}{d_{FN_F}}\right)\phi_F - \left(\frac{E'_f}{d_{CF}} + \delta_C \frac{T'_f}{d_{CN_C}}\right)\phi_C + \delta_C \frac{T'_f}{d_{CN_C}}\phi_{N_C} - \delta_F \frac{T'_f}{d_{FN_F}}\phi_{N_F}\end{aligned} \tag{17}$$

Again the weight factors are computed to obey relations similar to Eq. (13) yielding

$$\delta_C^{\bullet} = \frac{\phi_{N_F}}{d_{FN_F}} \Big/ \left(\frac{\phi_{N_C}}{d_{CN_C}} + \frac{\phi_{N_F}}{d_{FN_F}} \right) \quad \delta_F^{\bullet} = \frac{\phi_{N_C}}{d_{CN_C}} \Big/ \left(\frac{\phi_{N_C}}{d_{CN_C}} + \frac{\phi_{N_F}}{d_{FN_F}} \right) \tag{18}$$

Substituting Eq. (18) in Eq. (17), the final form of the fully linearized diffusion flux is obtained as

$$\overline{\nabla\phi_f} \cdot \boldsymbol{S}_f' = \left(\frac{E_f'}{d_{CF}} + \frac{\phi_{N_C} T_f'}{\phi_{N_C} d_{FN_F} + \phi_{N_F} d_{CN_C}} \right) \phi_F - \left(\frac{E_f'}{d_{CF}} + \frac{\phi_{N_F} T_f'}{\phi_{N_C} d_{FN_F} + \phi_{N_F} d_{CN_C}} \right) \phi_C \tag{19}$$

With this treatment, a fully implicit discretization of the diffusion term is obtained.

Satisfying the DMP

Experimentation with the MIND scheme revealed that satisfaction of the DMP is dependent on the type of elements used (quadrilateral or triangular), the quality and size of mesh, and the method adopted for calculating the gradient (Gaussian or least square). This is not surprising as the value of the constructed cross node ϕ_{N_C} or ϕ_{N_F} (i.e., Eq. (15)) heavily depends on the quality of the cell gradient used for its construction. Therefore, to guarantee fulfillment of the DMP, the gradient used in the calculation of ϕ_{N_C} or ϕ_{N_F} should be controlled by limiting its value, as it is usually done in the discretization of the convection term when using HR schemes [44–47]. Following this approach and denoting the limiter by ψ, Eq. (15) is modified to

$$\phi_{N_C} = \phi_C + \psi_C \nabla\phi_C \cdot \boldsymbol{d}_{CN_C} \quad \phi_{N_F} = \phi_F + \psi_F \nabla\phi_F \cdot \boldsymbol{d}_{FN_F} \tag{20}$$

The limiter adopted in this study is the one suggested by Venkatakrishnan [51, 52] and is given by

$$\psi = \frac{1}{\alpha} \left[\frac{\alpha\left(\beta^2 + \varepsilon^2\right) + 2\alpha^2\beta}{\beta^2 + 2\alpha^2 + \alpha\beta + \varepsilon^2} \right] \tag{21}$$

The expressions for α and β for the calculation of ϕ_{N_C} are defined as

$$\alpha = \phi_{N_C} - \phi_C \quad \beta = \begin{cases} \phi_{max} - \phi_C & \text{if } \alpha > 0 \\ \phi_{min} - \phi_C & \text{if } \alpha < 0 \end{cases} \tag{22}$$

where ϕ_{max} and ϕ_{min} are the maximum and minimum ϕ values at the C element and its immediate neighbors (ϕ_{N_F} can be calculated in a similar way). The value of the variable ε is computed as [53]

$$\varepsilon = \varepsilon' \left(\phi^{max} - \phi^{min} \right) \tag{23}$$

As suggested by Zang [53], ε' is a positive number less than 0.2 (a value of 0 is used in this work), while ϕ^{max} and ϕ^{min} are the maximum and minimum values of ϕ over the entire domain. Following this approach, the DMP is fully satisfied.

Treatment at a boundary face

A boundary element has at least one boundary face, which coincides with the domain border where boundary conditions are applied. In solving diffusion problems, the following four types of boundary conditions are commonly encountered [9]: (i) a specified value of the unknown variable (Dirichlet condition); (ii) a specified flux (von Neumann condition); (iii) a constitutive equation relating the unknown variable to the flux at the boundary (Robin condition); and (iv) a symmetry condition applicable along a symmetry plane.

Denoting by C the centroid of a boundary element and by b the centroid of its boundary face whose modified surface vector is $\boldsymbol{S}'_{\mathrm{b}}$ (Figure 3), then the discretization of the boundary flux for the different boundary condition types is as detailed next.

Dirichlet boundary condition

Along a Dirichlet boundary (Figure 3*a*), the value of the dependent variable ϕ_{b} is known while the flux is unknown and should be expressed in terms of ϕ_{C}. Following a Rhie–Chow-like interpolation [9], the gradient at the boundary face is written as

$$\nabla\phi_{\mathrm{b}} = \overline{\nabla\phi_{\mathrm{b}}} + \left(\frac{\phi_{\mathrm{b}} - \phi_{\mathrm{C}}}{d_{\mathrm{Cb}}} - \overline{\nabla\phi_{\mathrm{b}}} \cdot \boldsymbol{e}_{\mathrm{Cb}}\right)\boldsymbol{e}_{\mathrm{Cb}} \tag{24}$$

where $\overline{\nabla\phi_{\mathrm{b}}}$ represents the value of $\nabla\phi_{\mathrm{b}}$ obtained by interpolation and $\boldsymbol{e}_{\mathrm{Cb}}$ a unit vector in the direction of Cb. Using Eq. (24) and setting interpolated values at the face equal to values at the centroid of the boundary element (i.e, C), the diffusion flux at the boundary face becomes

$$\begin{aligned}\nabla\phi_{\mathrm{b}} \cdot \boldsymbol{S}'_{\mathrm{b}} &= \nabla\phi_{\mathrm{C}} \cdot \boldsymbol{S}'_{\mathrm{b}} + \left(\frac{\phi_{\mathrm{b}} - \phi_{\mathrm{C}}}{d_{\mathrm{Cb}}} - \nabla\phi_{\mathrm{C}} \cdot \boldsymbol{e}_{\mathrm{Cb}}\right)\underbrace{\boldsymbol{e}_{\mathrm{Cb}} \cdot \boldsymbol{S}'_{\mathrm{b}}}_{E'_{\mathrm{b}}} \\ &= \underline{\phi_{\mathrm{b}}\frac{E'_{\mathrm{b}}}{d_{\mathrm{Cb}}} + \phi_{\mathrm{N_C}}\frac{T'_{\mathrm{b}}}{d_{\mathrm{CN_C}}}} - \left(\frac{E'_{\mathrm{b}}}{d_{\mathrm{Cb}}} + \frac{T'_{\mathrm{b}}}{d_{\mathrm{CN_C}}}\right)\phi_{\mathrm{C}}\end{aligned} \tag{25}$$

The underlined term is treated explicitly. Since ϕ_{b} is known, the only explicit part is the one involving $\phi_{\mathrm{N_C}}$.

Von Neumann boundary condition

For this boundary condition (Figure 3*b*), usually the flux per unit area ($\mathrm{Flux_b}$) is specified. In the context of a FVM, this is a natural condition not requiring any specific treatment and its total value ($\mathrm{Flux_b S_b}$) is directly added as a source in the discretized equation. The value of the dependent variable

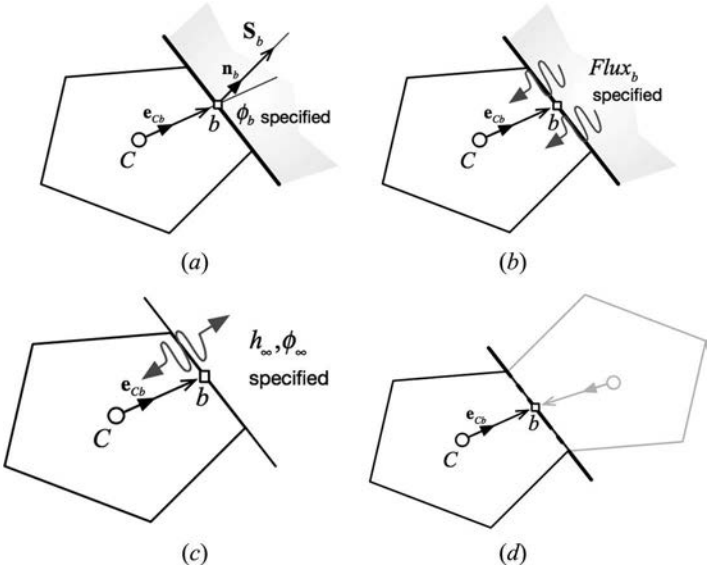

Figure 3. Boundary element with a boundary face subjected to (*a*) Dirichlet, (*b*) von Neumann, (*c*) Robin, and (*d*) symmetry boundary condition.

at the boundary, needed in calculating the gradient at the centroid of the boundary element, is computed iteratively from Eq. (25) as

$$\phi_b = \left[\mathrm{Flux}_b S_b + \left(\frac{E'_b}{d_{Cb}} + \frac{T'_b}{d_{CN_C}}\right)\phi_C - \phi_{N_C}\frac{T'_b}{d_{CN_C}}\right]\frac{d_{Cb}}{E'_b} \tag{26}$$

Robin boundary condition

For this condition (Figure 3*c*), information at the boundary is specified through a convection transfer coefficient h_∞ and a free stream value of the dependent variable ϕ_∞. The constitutive equation is derived by setting the convection flux at the boundary face equal to the diffusion flux and is given by

$$\mathrm{Flux}_b S_b = \phi_b\frac{E'_b}{d_{Cb}} + \phi_{N_C}\frac{T'_b}{d_{CN_C}} - \left(\frac{E'_b}{d_{Cb}} + \frac{T'_b}{d_{CN_C}}\right)\phi_C = h_\infty(\phi_\infty - \phi_b)S_b \tag{27}$$

Equation (27) yields the following expression for ϕ_b :

$$\phi_b = \left[\left(\frac{E'_b}{d_{Cb}} + \frac{T'_b}{d_{CN_C}}\right)\phi_C + h_\infty\phi_\infty S_b - \phi_{N_C}\frac{T'_b}{d_{CN_C}}\right] \Big/ \left(\frac{E'_b}{d_{Cb}} + h_\infty S_b\right) \tag{28}$$

Substituting the value of ϕ_b back in Eq. (27), the discretized flux at the face is obtained as

$$\nabla\phi_b \cdot \boldsymbol{S}'_b = \underline{\frac{h_\infty\phi_\infty S_b \frac{E'_b}{d_{Cb}}}{\frac{E'_b}{d_{Cb}} + h_\infty S_b} + \frac{T'_b}{d_{CN_C}}\left(1 - \frac{\frac{E'_b}{d_{Cb}}}{\frac{E'_b}{d_{Cb}} + h_\infty S_b}\right)\phi_{N_C}} - \left(\frac{E'_b}{d_{Cb}} + \frac{T'_b}{d_{CN_C}}\right)\frac{h_\infty S_b}{\frac{E'_b}{d_{Cb}} + h_\infty S_b}\phi_C \tag{29}$$

where the underlined term is treated explicitly.

Symmetry boundary condition

Since along symmetry boundary the normal flux of ϕ is zero (Figure 3*d*), a symmetry boundary condition is equivalent to a Von Neumann boundary condition with a zero flux. Thus the boundary flux is dropped from the discretized equation, while the value of ϕ_b is computed from Eq. (26) with Flux_b set to zero.

Test problems

To evaluate the performance and accuracy of the MIND scheme, a set of test problems involving a combination of nonorthogonal meshes and anisotropic coefficients are used. The MIND scheme is first validated and compared to the semi-implicit diffusion scheme on highly nonorthogonal grids with isotropic diffusion and then on two test problems involving anisotropic diffusion for grids of different skewness and density. The generated solutions are used to evaluate the robustness and accuracy of the MIND scheme for both quadrilateral and triangular elements. The fourth test case is used to demonstrate that the MIND scheme satisfies the DMP property. The last problem shows the correctness of the suggested treatment for the various boundary condition types. For all results reported in this paper, computations were continued until the maximum residual in the domain dropped below 10^{-8}.

Test 1: Isotropic diffusion in a highly nonorthogonal domain

In this first test, a simple isotropic diffusion validation problem is used to compare the accuracy of the MIND scheme with the semi-implicit implementation. A schematic of the physical domain is

displayed in Figure 4(*a*), with Dirichlet boundary conditions set on all boundaries and equal to

$$\phi = x + y + xy \tag{30}$$

The exact solution is also given by Eq. (30). The problem is solved using quadrilateral elements with grid systems of sizes 2^6, 2^8, 2^{10}, 2^{12}, 2^{14}, 2^{16}, and 2^{18} cells. The variations of the maximum and RMS errors with grid density for solutions generated using the MIND and SI schemes are displayed in Figure 4(*b*). The maximum and RMS errors are defined as

$$\text{Error}_{\text{MAX}} = \underset{i=1}{\overset{N}{\text{MAX}}} \left| \phi_{i,\text{exact}} - \phi_{i,\text{numerical}} \right| \quad \text{error}_{\text{RMS}} = \sqrt{\frac{\sum_{i=1}^{N} \left(\phi_{i,\text{exact}} - \phi_{i,\text{numerical}} \right)^2}{N}} \tag{31}$$

where N is the total number of elements used. As shown in Figure 6(*b*), the maximum and RMS errors generated using both schemes decrease with increasing mesh density and are almost identical indicating that MIND is as accurate as the SI scheme. Moreover, the variations of the maximum and RMS errors with number of elements presented in Figure 6(*b*), indicate that the solution is almost second-order accurate. This can be confirmed by noticing that N (the grid size) can be written as $N = L^2/\Delta x^2$, where L is the side of a square having the same area as the original domain and Δx^2 the average element area. Substituting in the equations shown in Figure 6(*b*) leads to $\text{Error}_{\text{max}} \propto \Delta x^{1.942}$ and $\text{RMS} \propto \Delta x^{1.956}$.

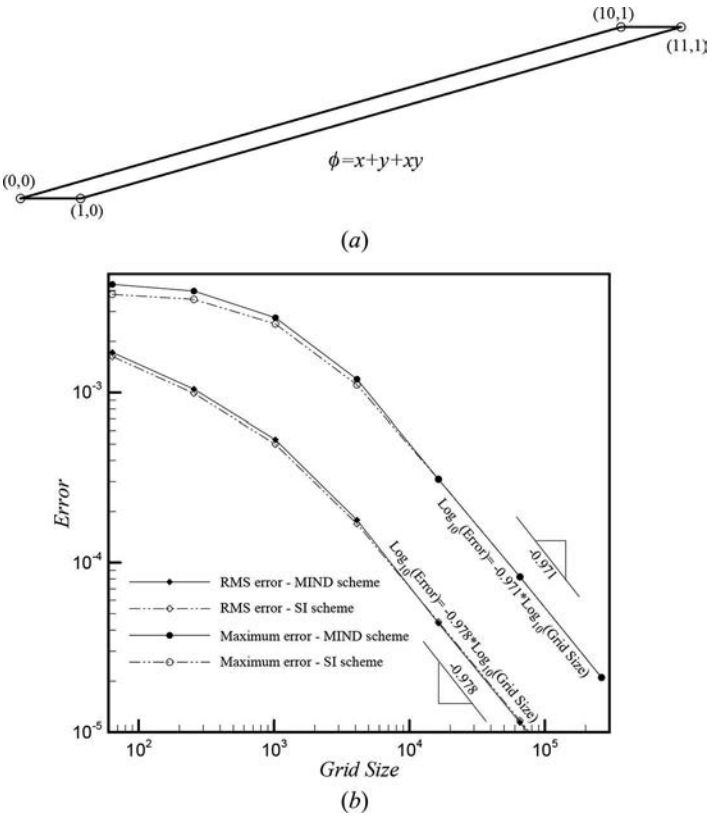

Figure 4. (*a*) Physical situation and (*b*) variation of RMS and maximum errors with a grid size using the MIND and SI schemes for the validation test case. *Note*: MIND, modified implicit nonlinear diffusion; SI, semi-implicit.

Test 2: Steady conduction with anisotropic coefficients

The second problem was devised by Keyhani and Polehn [54]. The physical situation, depicted in Figure 5(*a*) along with the boundary conditions, represents a square domain of side 1 with an orthotropic material having a nonzero conduction in the ξ-direction (i.e., $k_{\xi\xi} \neq 0$) and a zero conduction in the η-direction (i.e., $k_{\eta\eta} = 0$). The solution is one dimensional in the ξ direction. In the (x, y) coordinate system, the solution is two dimensional and is reported in [32, 54].

Solutions are obtained here for a diffusion tensor in the (x, y) coordinate system given by

$$\begin{pmatrix} k_{xx} & k_{xy} \\ k_{yx} & k_{yy} \end{pmatrix} = \begin{pmatrix} 1/4 & -\sqrt{3}/4 \\ -\sqrt{3}/4 & 3/4 \end{pmatrix} \tag{32}$$

The domain is discretized using both quadrilateral (structured grid) and triangular elements (unstructured grid). For the structured grid method, the problem is solved for seven mesh densities with values of 2^6, 2^8, 2^{10}, 2^{12}, 2^{14}, 2^{16}, and 2^{18} quadrilateral elements using Shestakov-type grids [55]. For each mesh size, the skewness factor α was varied between 0.5 and 0.325, with the value 0.5 resulting in an orthogonal Cartesian grid. Examples of the mesh systems used are displayed in Figure 5 for a grid with size of 2^{12} elements and for values of α equal to 0.45 (Figure 5*b*), 0.4 (Figure 5*c*), 0.35 (Figure 5*d*), and 0.325 (Figure 5*e*). As shown, the grid skewness increases as α decreases. Solutions are obtained using both the MIND and the SI schemes.

The effect of grid skewness on the accuracy of the MIND scheme is demonstrated in Figure 6 by comparing, on the densest grid, the ϕ-contours generated numerically with similar ones obtained from the exact solution for different values of the skewness factor α. As shown in Figures 6(*a*)–6

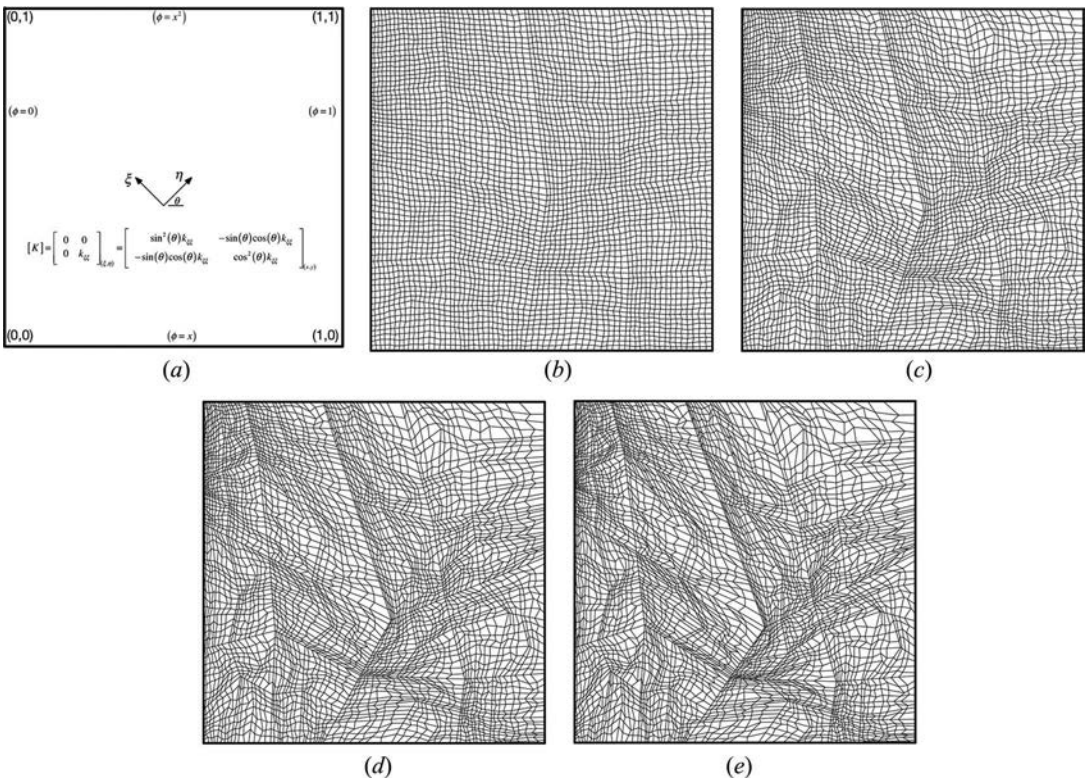

Figure 5. (*a*) Physical situation and boundary conditions for anisotropic diffusion in a square domain with an orthotropic material; (b–e) Shestakov-type grid systems using 2^{12} elements with (*b*) α = 0.45, (*c*) α = 0.4, (*d*) α = 0.35, and (*e*) α = 0.325.

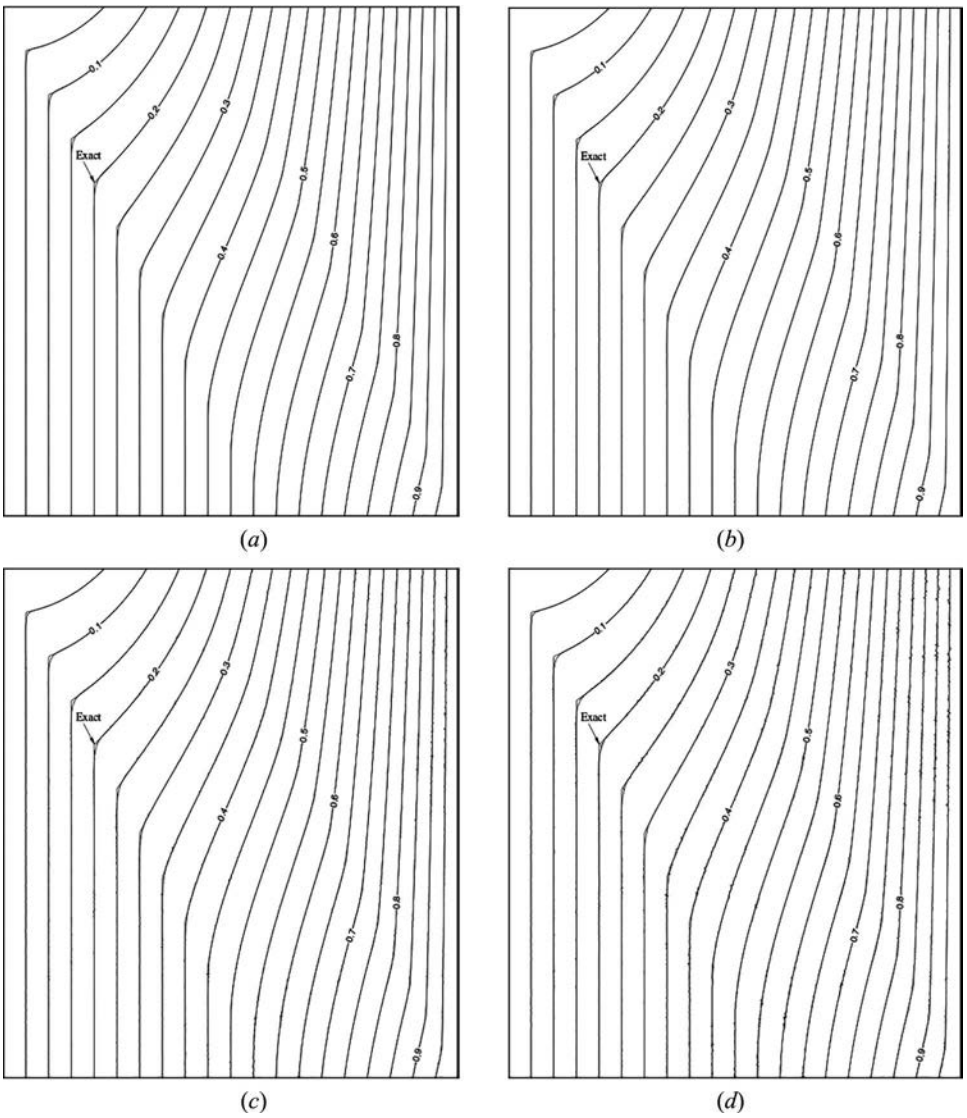

Figure 6. Comparison of ϕ-contours generated numerically on a grid with size of 2^{18} elements with similar ones obtained from the exact solution for (*a*) $\alpha = 0.45$, (*b*) $\alpha = 0.40$, (*c*) $\alpha = 0.35$, and (*d*) $\alpha = 0.325$.

(*d*), for $\alpha = 0.45, 0.4, 0.35,$ and 0.325, respectively, both solutions are on top of each other with the effect of grid skewness being almost nonexisting.

In solving the problem, no under-relaxation was required with the MIND scheme except on the densest grid for $\alpha = 0.325$. On the other hand, to promote convergence with the SI scheme under-relaxation was used for many of the cases with the value of the under-relaxation factor decreasing as the grid density increases and/or the skewness factor decreases. In fact, it was not possible to reduce the residuals below 3.8×10^{-5} with the SI scheme on the densest grid for $\alpha = 0.325$. This behavior of the SI scheme is due to the explicit treatment of the nonorthogonal part of the diffusion flux whose contribution to the total flux increases as the grid skewness increases.

The robustness and higher rate of convergence of the MIND scheme are demonstrated through the residual history plots presented in Figure 7. For a skewness factor $\alpha = 0.4$, plots show the reduction in the maximum absolute residuals [9] with iteration on grids with sizes of 2^{12} (Figure 7*a*),

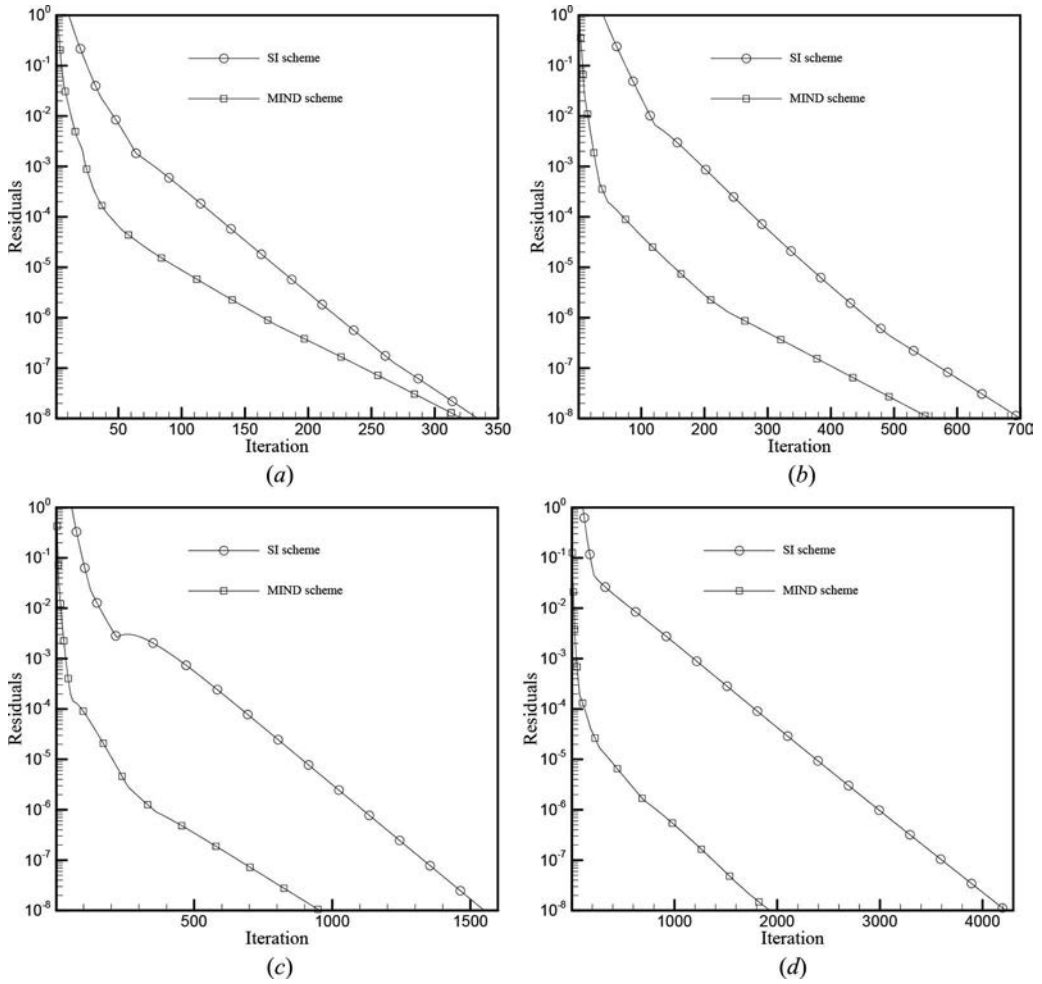

Figure 7. Reduction of residuals with iterations for the numerical solution of anisotropic diffusion in a square domain with an orthotropic material using the MIND and SI schemes over Shestakov-type grid systems of skewness factor $\alpha = 0.4$ and with sizes of (*a*) 2^{12}, (*b*) 2^{14}, (*c*) 2^{16}, and (*d*) 2^{18} quadrilateral elements. *Note*: MIND, modified implicit nonlinear diffusion; SI, semi-implicit.

2^{14} (Figure 7*b*), 2^{16} (Figure 7*c*), and 2^{18} (Figure 7*d*). For all grid sizes, the MIND scheme requires lower number of iterations to reach convergence than the SI scheme. As shown, the difference in the required number of iterations between the two schemes increases as the grid size increases.

The maximum and RMS errors for all cases studied with MIND and the SI schemes, which are computed according to Eq. (31), are displayed in Figures 8(*a*) and 8(*b*), respectively. As shown, results are plotted as a function of the grid size for different values of α. As expected, both the RMS (Figure 8*a*) and maximum (Figure 8*b*) errors decrease with increasing grid density. For this problem, the effect of increasing grid skewness is seen to have a favorable effect at low grid density, where the maximum and RMS errors are seen to decrease with decreasing α. This is attributed to accidently having more grid points concentrated in important regions of the domain where higher gradients exist. This advantage fade away as the grid density increases indicating that enough points are clustered in these regions even with a uniform grid (i.e., for $\alpha = 0.5$). Consistently, the MIND scheme is seen to be more accurate than the SI scheme for all values of α used with the difference in error between the two schemes decreasing as the grid size increases. This better performance of the MIND scheme is more apparent with the maximum error shown in Figure 8(*b*) than the RMS error presented in Figure 8(*a*).

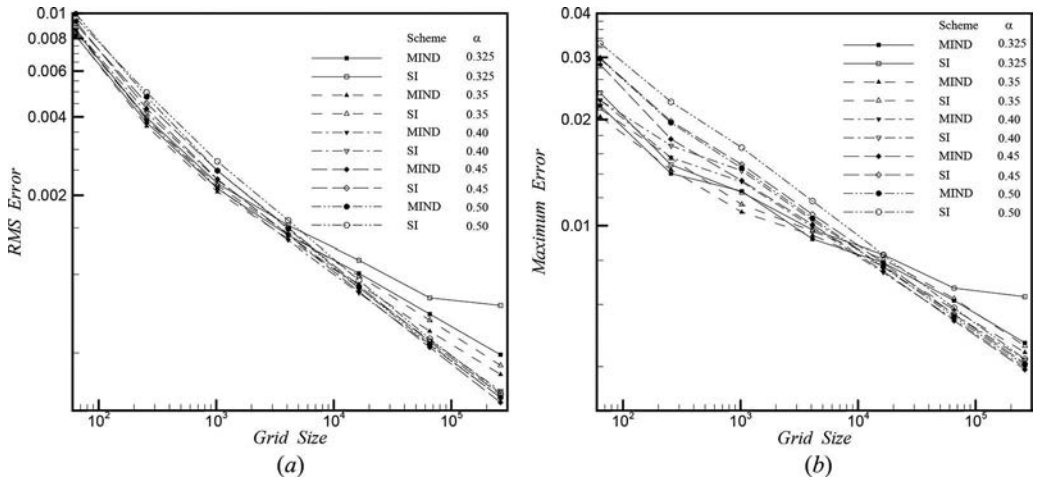

Figure 8. Variation of (*a*) RMS and (*b*) maximum errors with a grid size for different values of α using the MIND and SI schemes for anisotropic diffusion in a square domain with an orthotropic material. *Note*: MIND, modified implicit nonlinear diffusion; SI, semi-implicit.

Results generated using unstructured grids are presented in Figures 9 and 10. Again the problem is solved using both the MIND and SI schemes for different mesh systems with sizes of 10^4, 3×10^4, 5×10^4, 10^5, 2×10^5, and 3×10^5 triangular elements. An illustrative mesh network used is depicted

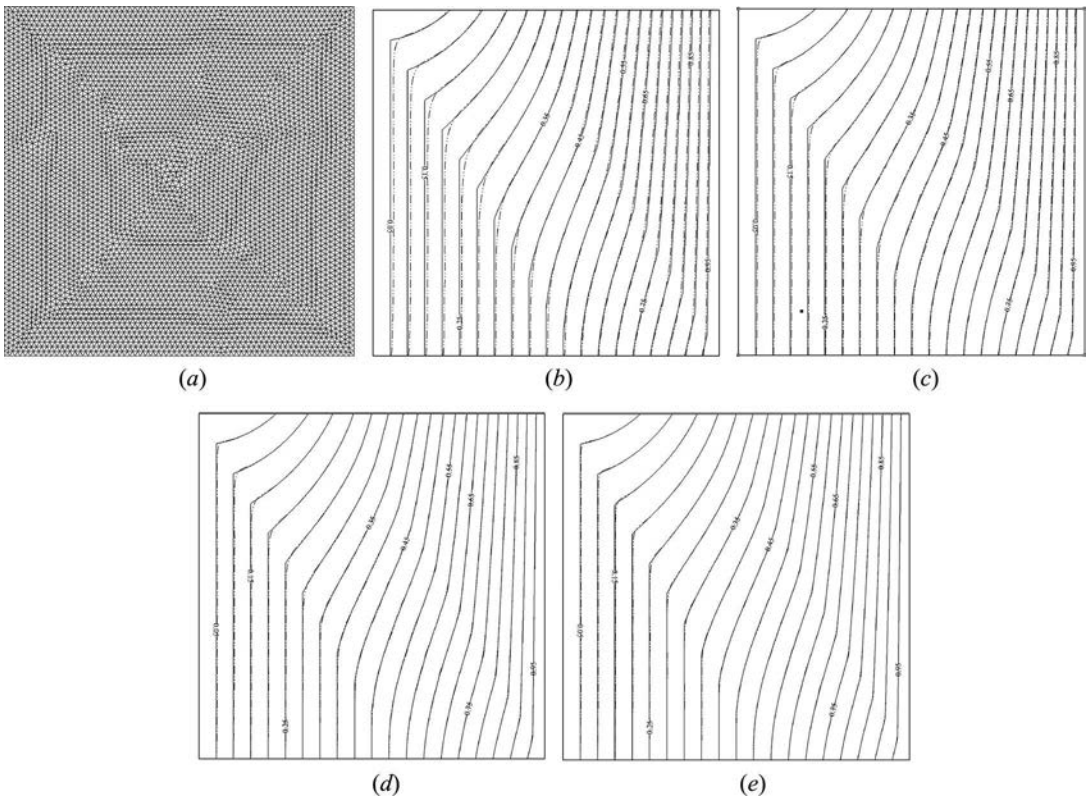

Figure 9. (*a*) Unstructured grid network with triangular elements; Comparison of φ-contours obtained from the exact solution with similar ones generated numerically using the MIND scheme for grid systems with sizes of (*b*) 10^4 elements, (*c*) 5×10^4 elements, (*d*) 10^5 elements, and (*e*) 3×10^5 elements. *Note*: MIND, modified implicit nonlinear diffusion.

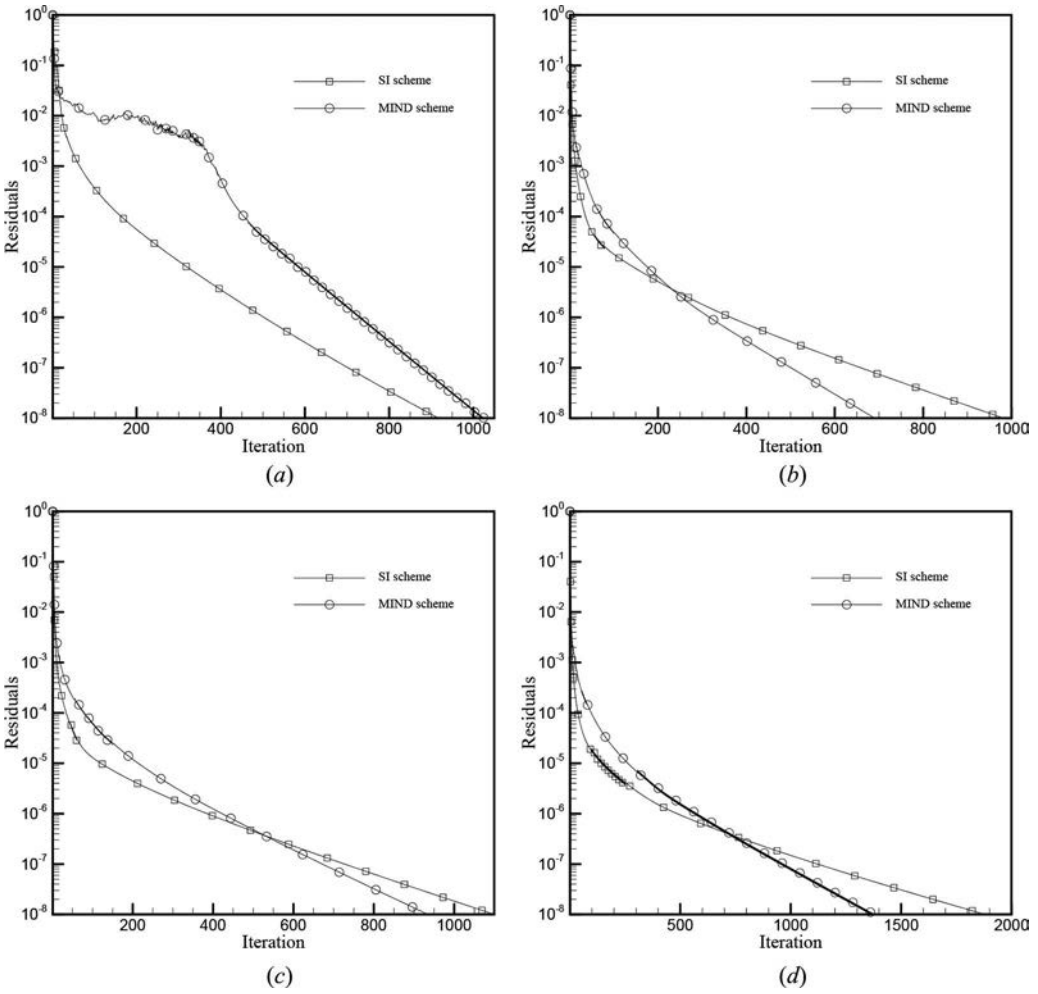

Figure 10. Reduction of residuals with iterations for the numerical solution of anisotropic diffusion in a square domain with an orthotropic material using the MIND and SI schemes over unstructured grid systems with sizes of (*a*) 3×10^4, (*b*) 5×10^4, (*c*) 10^5, and (*d*) 2×10^5 triangular elements. *Note*: MIND, modified implicit nonlinear diffusion; SI, semi-implicit.

in Figure 9(*a*). Comparisons of ϕ-contours obtained numerically using the MIND scheme with similar ones obtained from the exact solution are depicted in Figures 9(*b*)–9(*e*) for grids with sizes of 10^4, 5×10^4, 10^5, and 3×10^5 triangular elements, respectively. As can be inferred from the plots, the numerical solution is very close to the exact solution even for the coarse grid (Figure 9*b*) with its accuracy increasing as the mesh size increases (Figures 9*c* and 9*d*) to fall almost on top of the analytical solution for the densest grid network used (Figure 9*e*).

Figure 10 compares the performance of the MIND scheme with the SI scheme by plotting, for both schemes, the reduction in residuals with iterations for grids with sizes of 3×10^4 (Figure 10*a*), 5×10^4 (Figure 10*b*), 10^5 (Figure 10*c*), and 2×10^5 (Figure 10*d*) triangular elements. Except for the coarsest grid (i.e., Figure 10*a*), the rate of convergence of the MIND scheme is higher than the rate of convergence of the SI scheme requiring lower number of iterations to reach the desired level of convergence. Whereas no under-relaxation is required for convergence with the MIND scheme, it is essential with the SI scheme. It is the combined effects of under-relaxation and explicit treatment of the nonorthogonal term that slows down the rate of convergence of the SI scheme.

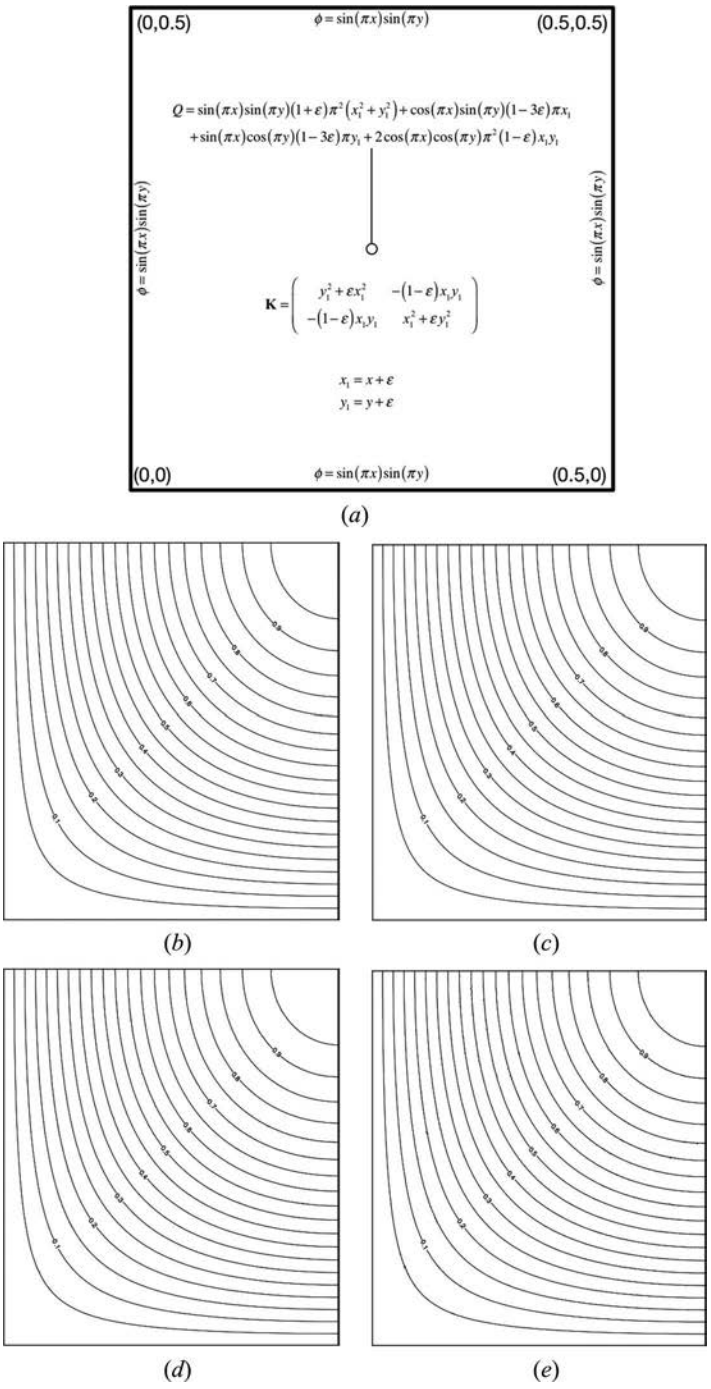

Figure 11. (*a*) Physical situation and boundary conditions for anisotropic diffusion in a square domain with a distributed source term; (*b*)–(*e*) Comparison of ϕ-contours generated numerically for an anisotropic ratio of 10^7 ($\varepsilon = 10^{-7}$) on a grid with size of 2^{18} elements with similar ones obtained from the exact solution for (*a*) $\alpha = 0.45$, (*b*) $\alpha = 0.40$, (*c*) $\alpha = 0.35$, and (*d*) $\alpha = 0.325$ for the anisotropic conduction with a distributed source term problem.

Test 3: Anisotropic conduction with a distributed source term

This case was used by several researchers [10, 35, 36, 40] for testing their discretization procedures to the locking problem and is used here for the same purpose. A schematic of the physical domain is

depicted in Figure 11(*a*) and represents a square of side 0.5. The conservation equation governing the problem is given by Eq. (1) with the expressions for both $\boldsymbol{K}$ and Q displayed in Figure 11(*a*). The problem is solved subject to the following Dirichlet boundary condition applied on all boundaries:

$$\phi = \sin(\pi x)\sin(\pi y) \tag{33}$$

The analytical solution for the problem is also given by Eq. (33). Again predictions are generated on structured and unstructured grid systems using quadrilateral and triangular elements, respectively.

The same structured grid systems used in the previous problem are used here, i.e., Shestakov-type grids [55] with sizes of 2^6, 2^8, 2^{10}, 2^{12}, 2^{14}, 2^{16}, and 2^{18} quadrilateral elements and for each grid size five mesh systems of different skewness. Solutions are obtained for two values of the parameter ε set to 10^{-3} and 10^{-7}. The anisotropic ratios for these two cases are 10^3 and 10^7, respectively. Results are presented in Figures 11–13. A comparison of the ϕ-contours generated numerically using the MIND scheme for $\varepsilon = 10^{-7}$ (i.e., the largest anisotropic ratio) on the densest grid system with similar ones obtained from the exact solution is presented in Figure 11(*b*) for $\alpha = 0.45$, Figure 11(*c*) for $\alpha = 0.4$, Figure 11(*d*) for $\alpha = 0.35$, and Figure 11(*e*) for $\alpha = 0.325$. As shown, in all cases both solutions fall on top of each other.

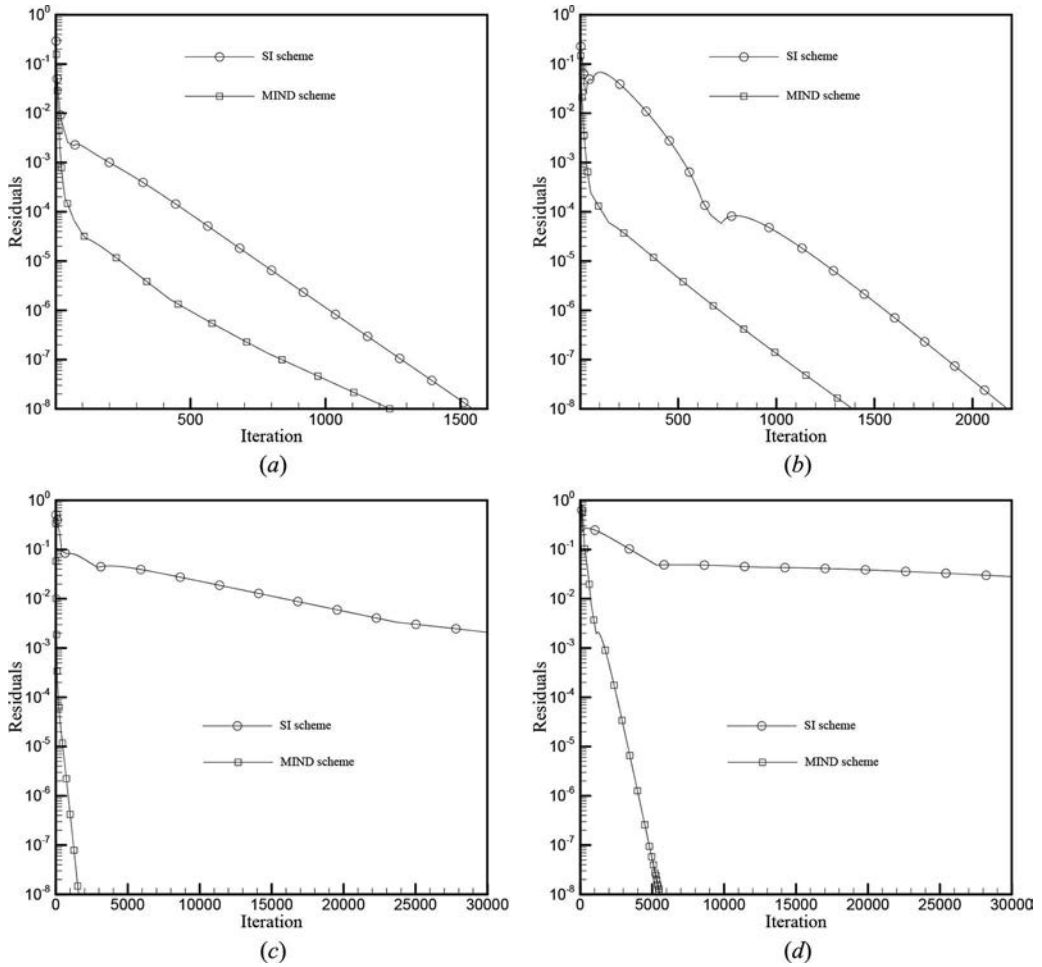

Figure 12. Reduction of residuals with iterations for the numerical solution of anisotropic diffusion in a square domain with a distributed source term using the MIND and SI schemes ($\varepsilon = 10^{-5}$) over Shestakov-type grid systems of size 2^{16} quadrilateral elements and for a skewness factor with the value of (*a*) $\alpha = 0.45$, (*b*) $\alpha = 0.4$, (*c*) $\alpha = 0.35$, and (*d*) $\alpha = 0.325$. *Note*: MIND, modified implicit nonlinear diffusion; SI, semi-implicit.

The effect of grid skewness on the convergence rate of both schemes is presented in Figure 12 for a grid with size of 2^{16} quadrilateral elements. Residuals are presented for grid systems with skewness factor values of 0.45 (Figure 12*a*), 0.40 (Figure 12*b*), 0.35 (Figure 12*c*), and 0.325 (Figure 12*d*). The higher convergence rate of the newly developed MIND scheme in comparison with the SI scheme is clear with its performance being by far better at low values of the skewness factor. For $\alpha = 0.35$ and 0.325, residuals for the SI scheme are presented for the first 30,000 iterations only (Figures 12*c* and 12*d*), since over a million iterations are required for convergence to be reached. On the other hand, convergence with the MIND scheme is obtained in 1,500 iterations for $\alpha = 0.35$ and 5,500 iterations for $\alpha = 0.325$.

The RMS and maximum solution errors for all cases studied using both the MIND and SI schemes are presented in Figure 13 for both values of ε considered. The RMS errors are displayed in Figures 13 (*a*) and 13(*c*) and the maximum errors in Figures 13(*b*) and 13(*d*). The trend of results is similar for both values of ε and indicates that the RMS and maximum errors decrease with increasing grid density and/or decreasing grid skewness. Numerical errors associated with both schemes are very close to each other confirming the accuracy of the newly developed MIND scheme. Depending on

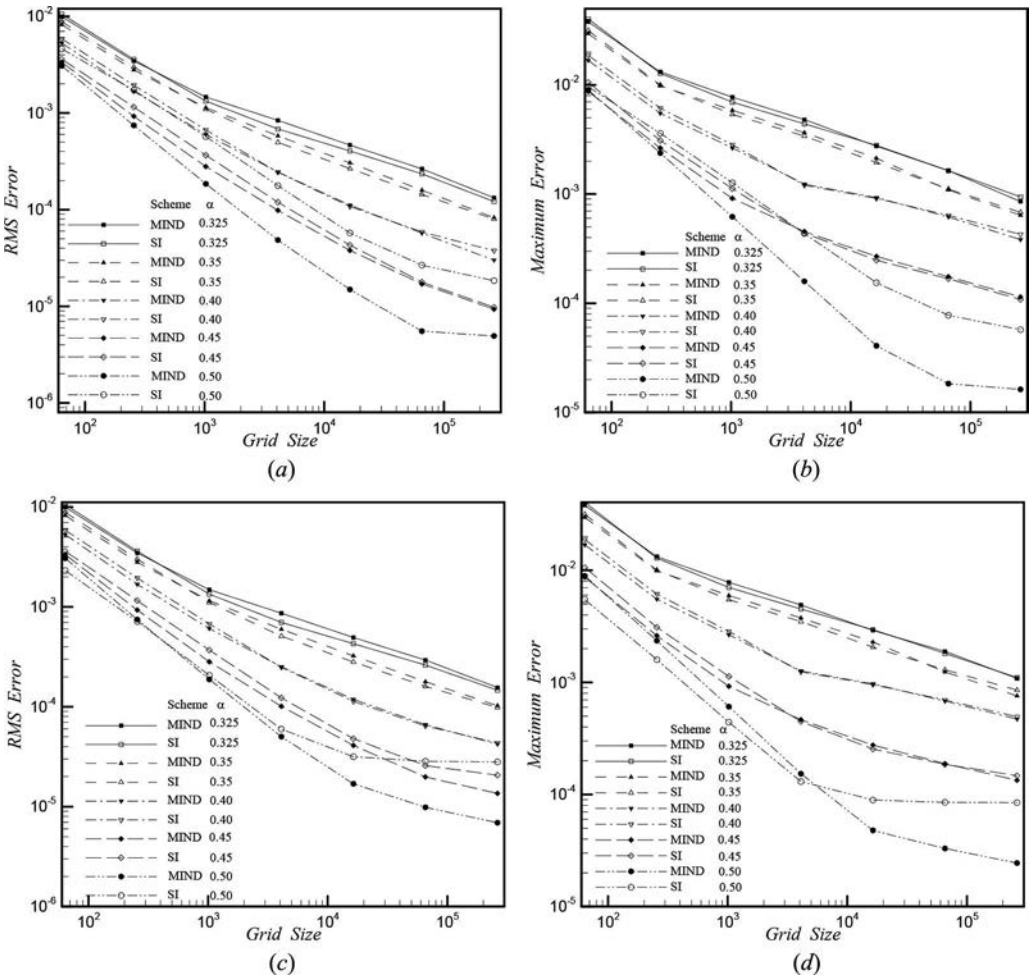

Figure 13. Variation of RMS (a, c) and maximum (b, d) errors with a grid size for different values of α and for ε values of 10^{-3} (*a, b*) and 10^{-7} (*c, d*) using the MIND and SI schemes for anisotropic diffusion in a square domain with a distributed sources term. *Note*: MIND, modified implicit nonlinear diffusion; SI, semi-implicit.

the case solved, the numerical error resulting from the MIND scheme may be either slightly lower or slightly higher than the one resulting from the SI scheme with no clear trend.

For unstructured grids, results generated with the MIND and SI schemes are displayed in Figures 14 and 15 for $\varepsilon = 10^{-7}$. Six grid systems with sizes of 10^4, 3×10^4, 5×10^4, 10^5, 2×10^5, and 3×10^5 triangular elements are used, exemplified by the grid shown in Figure 14(*a*). A comparison of ϕ-contours predicted using the MIND scheme with similar ones obtained from the exact solution are depicted in Figures 14(*b*)–14(*e*) for grids with sizes of 10^4, 5×10^4, 10^5, and 3×10^5 triangular elements, respectively. For all grid sizes, numerical solutions are very close to the analytical ones with their accuracy increasing as the mesh size increases and both solutions are almost identical on the densest grid used.

The higher rate of convergence of the MIND scheme as compared to the SI scheme can be inferred from the plots displayed in Figure 15. Results show the reduction in residuals with iteration for solutions obtained with the MIND and SI schemes using grids with sizes of 3×10^4 (Figure 15*a*), 5×10^4 (Figure 15*b*), 10^5 (Figure 15*c*), and 2×10^5 (Figure 15*d*) triangular elements. As shown, the rate of convergence of the MIND scheme is always higher than the rate of convergence of the SI scheme for the same reasons stated earlier. As shown, the solution is fully bounded satisfying the DMP.

Test 4: Anisotropic conduction in a hollow cylinder

A schematic of the physical domain is shown in Figure 16(*a*). The domain is circular in shape of diameter 1 with a central circular hole of diameter 1/15. A similar problem of square hollow duct was studied in [56] to evaluate the boundedness of the discretization procedure. The anisotropic

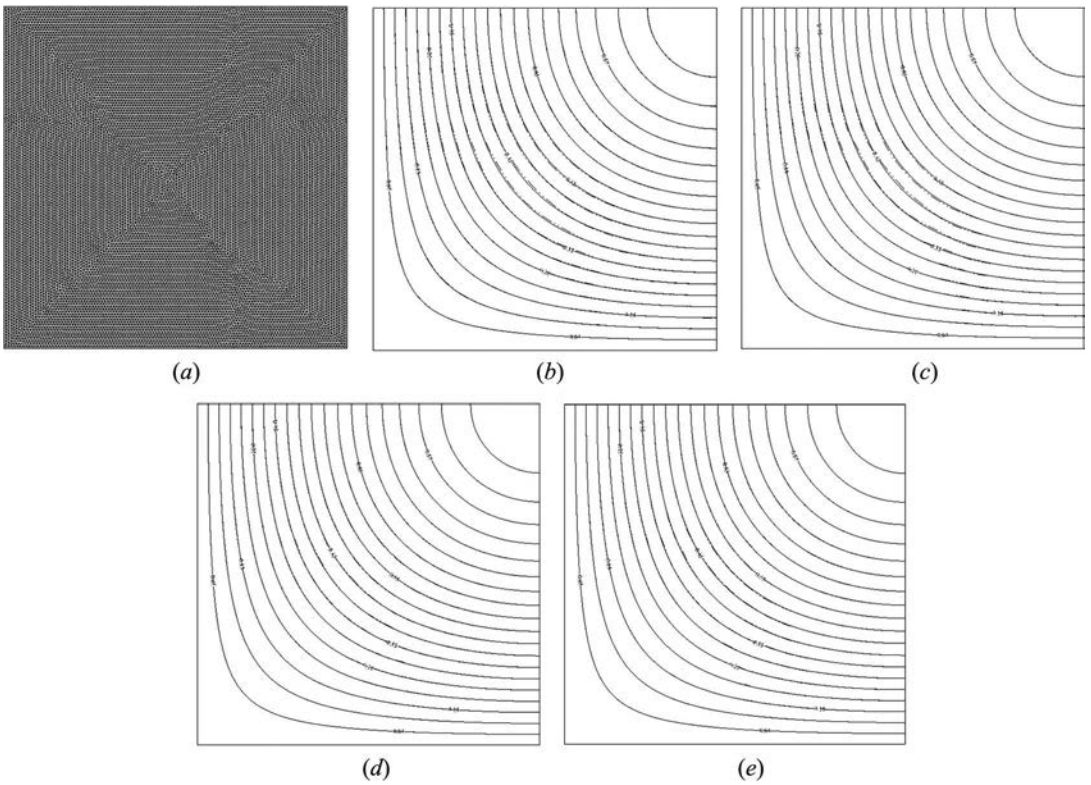

Figure 14. (*a*) Unstructured grid network with triangular elements; Comparison of ϕ-contours obtained from the exact solution with similar ones generated numerically using the MIND scheme for grid systems with sizes of (*b*) 10^4 elements, (*c*) 5×10^4 elements, (*d*) 10^5 elements, and (*e*) 3×10^5 elements. *Note*: MIND, modified implicit nonlinear diffusion.

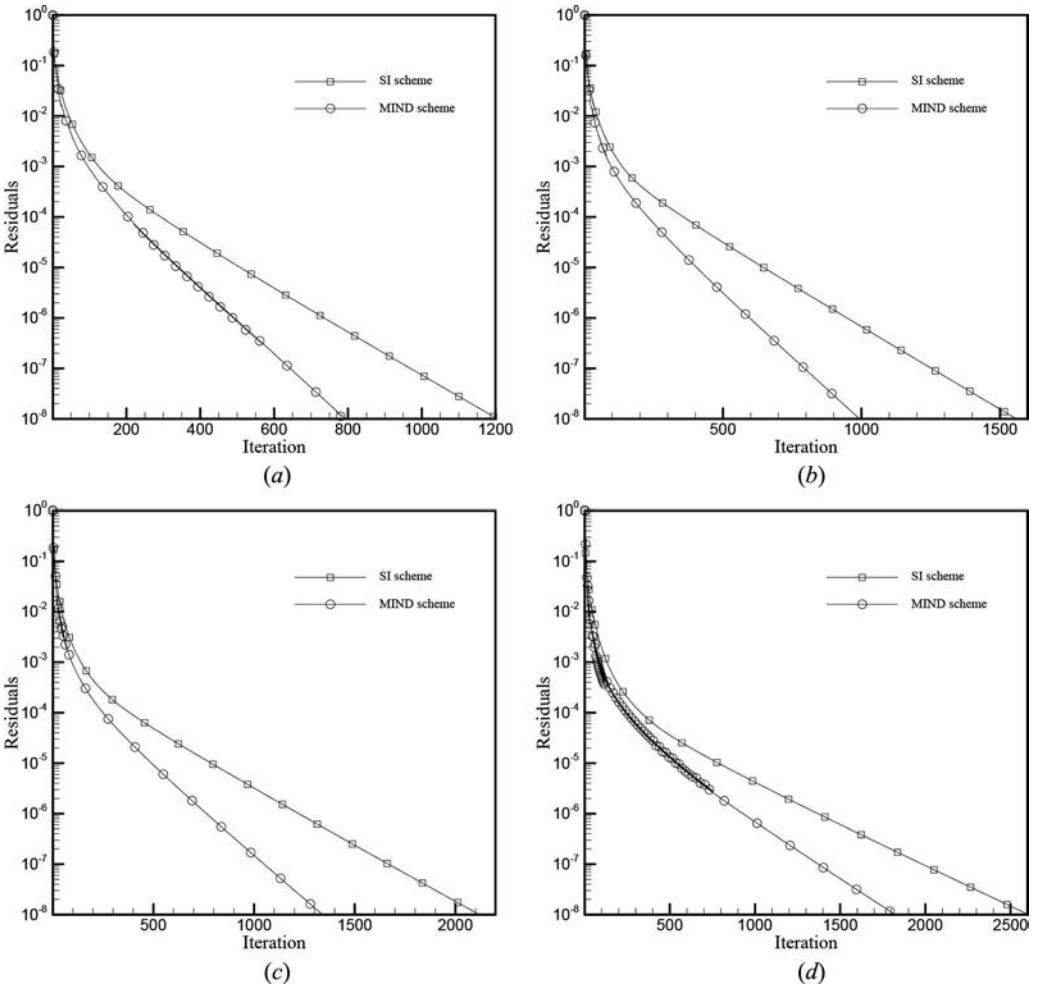

Figure 15. Reduction of residuals with iterations for the numerical solution of anisotropic diffusion in a square domain with a distributed source term using the MIND and SI schemes over unstructured grid systems with sizes of (*a*) 3×10^4, (*b*) 5×10^4, (*c*) 10^5, and (*d*) 2×10^5 triangular elements. *Note*: MIND, modified implicit nonlinear diffusion; SI, semi-implicit.

conductivity tensor is obtained by rotation of the diagonal diffusion tensor ($k_{\eta\eta} = 1$, $k_{\xi\xi} = \varepsilon$, $k_{\eta\xi} = k_{\xi\eta} = 0$) through an angle θ and is given by

$$\boldsymbol{K}_{(x,y)} = \begin{pmatrix} \cos^2(\theta) + \varepsilon \sin^2(\theta) & (1-\varepsilon)\sin(\theta)\cos(\theta) \\ (1-\varepsilon)\sin(\theta)\cos(\theta) & \sin^2(\theta) + \varepsilon\cos^2(\theta) \end{pmatrix} \tag{34}$$

The problem is solved for $\varepsilon = 100$ and $\theta = -\pi/6$ while enforcing a Dirichlet condition of $\phi_{\min} = 1$ on the outer boundaries and $\phi_{\max} = 3$ on the inner boundaries. Two sets of results (with and without limiting the values of ϕ_{N_C} and ϕ_{N_F}) over four grid densities with values of 2^{12}, 2^{14}, 2^{16}, and 2^{18} quadrilateral elements for structured grid are generated. An illustrative grid network is depicted in Figure 16(*b*). No analytical solution is available for the problem, but its lower limit is $\phi = \phi_{\min}$ and its upper limit is $\phi = \phi_{\max}$ and is used here to check whether the DMP is satisfied. The ϕ-contours over the domain generated using the MIND scheme with and without limiting the values of ϕ_{N_C} and ϕ_{N_F} are compared in Figures 16(*c*)–16(*f*) for the various grid systems used. The minimum and maximum predicted ϕ values over the domain with each grid size are also displayed. As shown, for grid densities

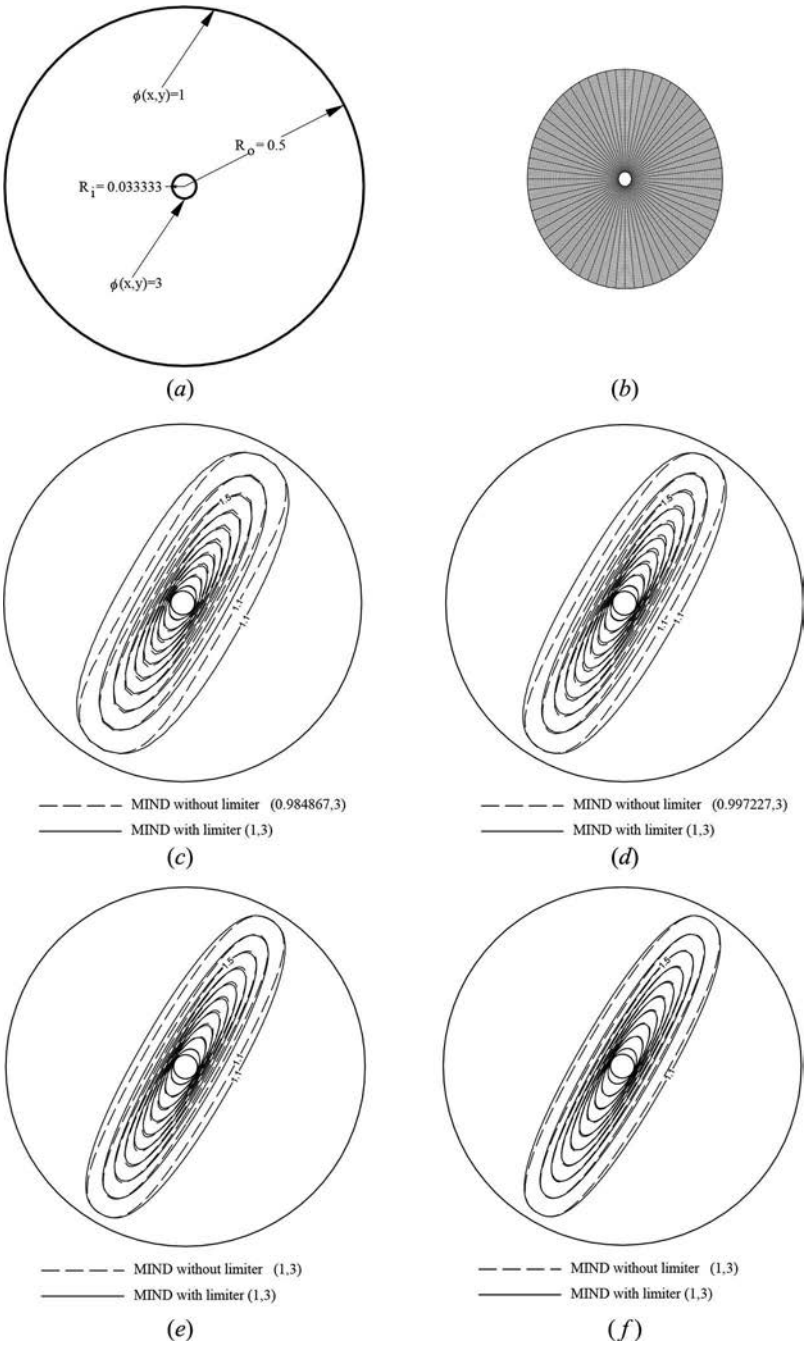

Figure 16. (*a*) Physical situation and boundary conditions for the anisotropic conduction in a hollow cylinder problem; (*b*) an illustrative grid network with quadrilateral elements used; (c–f) comparison of ϕ-contours generated numerically using the MIND scheme with and without a limiter for $\varepsilon = 100$ over grid systems with sizes of (*c*) 2^{12}, (*d*) 2^{14}, (*e*) 2^{16}, and (*f*) 2^{18} quadrilateral elements. *Note*: MIND, modified implicit nonlinear diffusion.

with sizes of 2^{12} (Figure 16*c*) and 2^{14} (Figure 16*d*) elements, the solution does not satisfy the DMP unless the values of ϕ_{N_C} and ϕ_{N_F} are limited. On the other hand, for denser grids with values of 2^{16} (Figure 16*e*) and 2^{18} (Figure 16*f*) elements, the DMP is satisfied with and without the use of a

limiter. Therefore, by limiting the values of ϕ_{N_C} and ϕ_{N_F} the DMP is always satisfied. Further it should be clarified that results were also generated for different values of ϕ_{min} and ϕ_{max} with the difference between them reaching a value as high as 10^5 and in all cases the DMP was found to be always satisfied. These results are not shown for compactness. The effect of using a limiter on the ϕ field can be inferred from the comparison of the contour plots presented in Figures 16(*a*)–16(*d*). Contours are very close to each other with the ones obtained when the limiter is activated being slightly more diffusive especially in the region where the value of ϕ is close to its lowest value (i.e., close to 1). The difference decreases as the grid density increases. This effect is similar to false diffusion associated with the use of upwind-biased convection schemes.

Plots in Figure 17 indicate that, for the various grid densities, using a limiter has a positive impact on the rate of convergence, reducing the number of iterations required to decrease the residuals to a desired level. This reduction is seen to be nearly independent of the grid size used (compare plots in Figures 17(*a*)–17(*d*)).

Solutions are generated also using unstructured grid networks with sizes of 10^3, 4×10^3, 15×10^3, and 65×10^3 triangular elements and results are reported in Figure 18. An illustration of the unstructured grid network used is depicted in Figure 18(*a*). The problem is solved for an

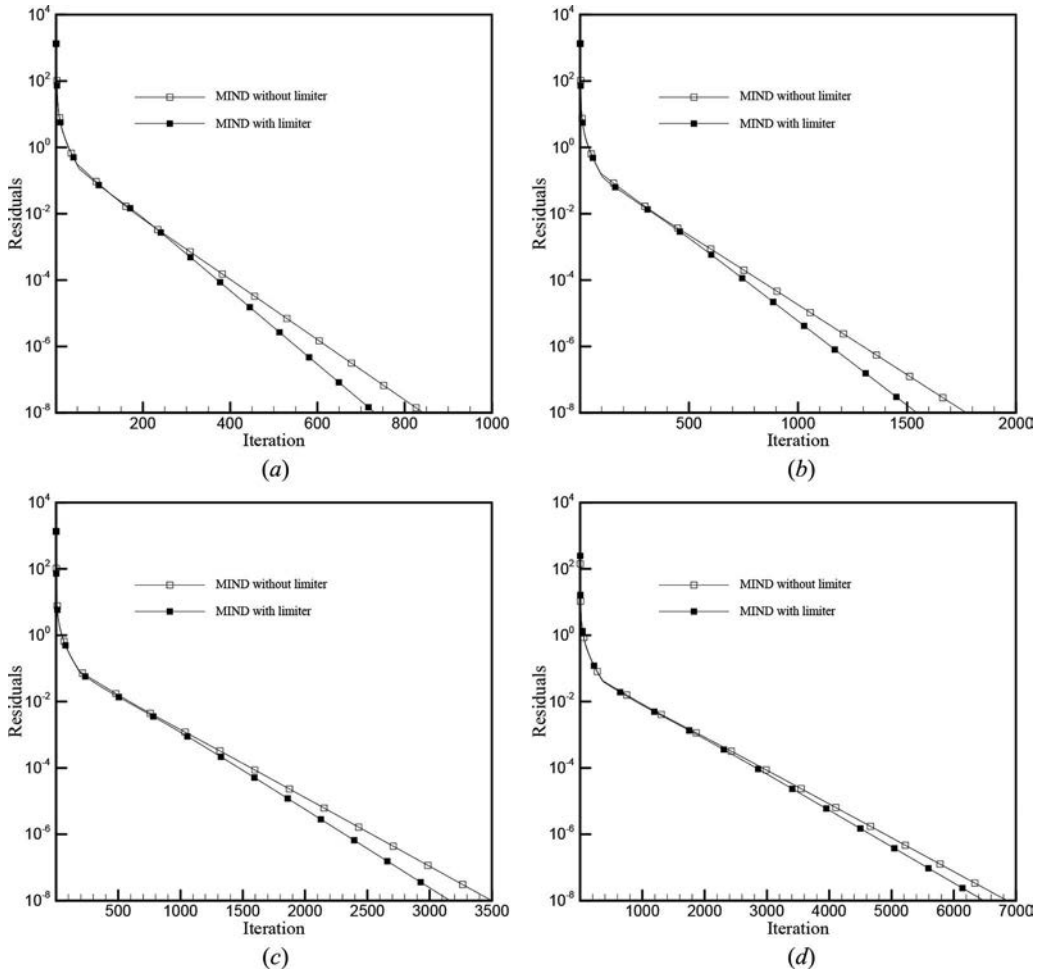

Figure 17. Reduction of residuals with iterations for the numerical solution of conduction in a hollow cylinder problem with $\varepsilon = 100$ using the MIND scheme with and without a limiter over Cartesian grid systems with sizes of (*a*) 2^{12}, (*b*) 2^{14}, (*c*) 2^{16}, and (*d*) 2^{18} quadrilateral elements. *Note*: MIND, modified implicit nonlinear diffusion.

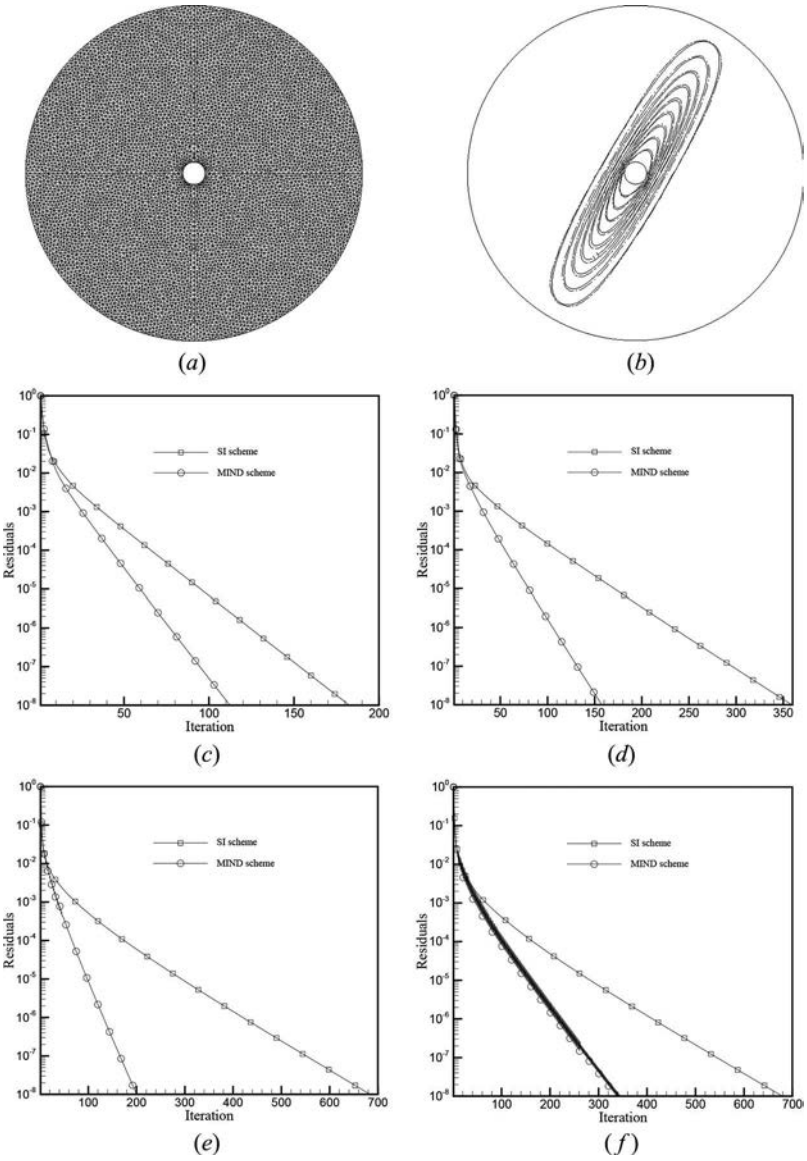

Figure 18. (*a*) Unstructured grid network with triangular elements; (*b*) Comparison of ϕ-contours for the anisotropic conduction in a hollow cylinder problem ($\varepsilon = 100$) generated numerically on a grid with the size of 1.5×10^4 triangular elements with similar ones obtained also numerically on a grid with the size of 6.5×10^4 triangular elements; Reduction of residuals with iterations using the MIND and SI schemes over unstructured grid systems with sizes of (*c*) 10^3, (*d*) 4×10^3, (*e*) 1.5×10^4, and (*f*) 6.5×10^4 triangular elements. *Note*: MIND, modified implicit nonlinear diffusion; SI, semi-implicit.

anisotropic ratio with value of 1/100. The densest grid solution obtained with the MIND scheme is considered to represent the exact solution with which other numerical solutions generated on coarser grids are compared. Such comparison is displayed in Figure 18(*b*) for a mesh with size of 15×10^3 triangular elements. As shown, solution approaches the exact one as the grid size increases. Again the convergence history plots presented in Figures 18(*c*)–18(*f*) confirm once more the higher rate of convergence of the MIND scheme in comparison with the SI scheme for all grid sizes used. Predictions obtained using the MIND scheme with the gradient calculated through the least squares method were found to satisfy the DMP for all grid sizes without the need for using a limiter.

Test 5: Anisotropic conduction with point sources

The purpose of the problem is to check the validity of the suggested treatment for the various boundary condition types. The physical situation is depicted in Figure 19(*a*) and represents the conduction of a property ϕ in a square domain of side $L = 10$. The domain is made of material with a diffusion coefficient tensor $\boldsymbol{K}$ given by

$$\boldsymbol{K} = \begin{pmatrix} 7.7 & -2.078 \\ -2.078 & 10.1 \end{pmatrix} \tag{35}$$

The problem is solved for the distribution of ϕ over the domain in the presence of point sources at the five locations shown in Figure 19(*a*). Two types of boundary conditions are used. In both, the lower and upper walls are maintained at $\phi = 273$ and $\phi = 373$, respectively. The difference in boundary conditions is along the side walls, where either a von Neumann condition with zero flux along the west and east walls is used or a mixed/Robin-type condition is applied with $\phi_\infty = 600$ and $h_\infty = 20$ along the west wall and $\phi_\infty = 300$ and $h_\infty = 10$ along the east wall. Results are generated using both the MIND and SI schemes on seven different grid sizes with values of 2^6, 2^8, 2^{10}, 2^{12}, 2^{14}, 2^{16}, and 2^{18} quadrilateral elements. For all grids, predictions obtained with both schemes are on top of each other. Maps of contour lines generated with both schemes on the densest grid are compared in Figures 19(*b*) and 19(*c*) for the von Neumann and Robin-type boundary condition, respectively. As shown, results generated with the MIND and SI scheme are indistinguishable confirming again the correctness of the MIND scheme. This is further revealed by the comparison of the fluxes presented in Figures 19(*d*)–19(*f*).

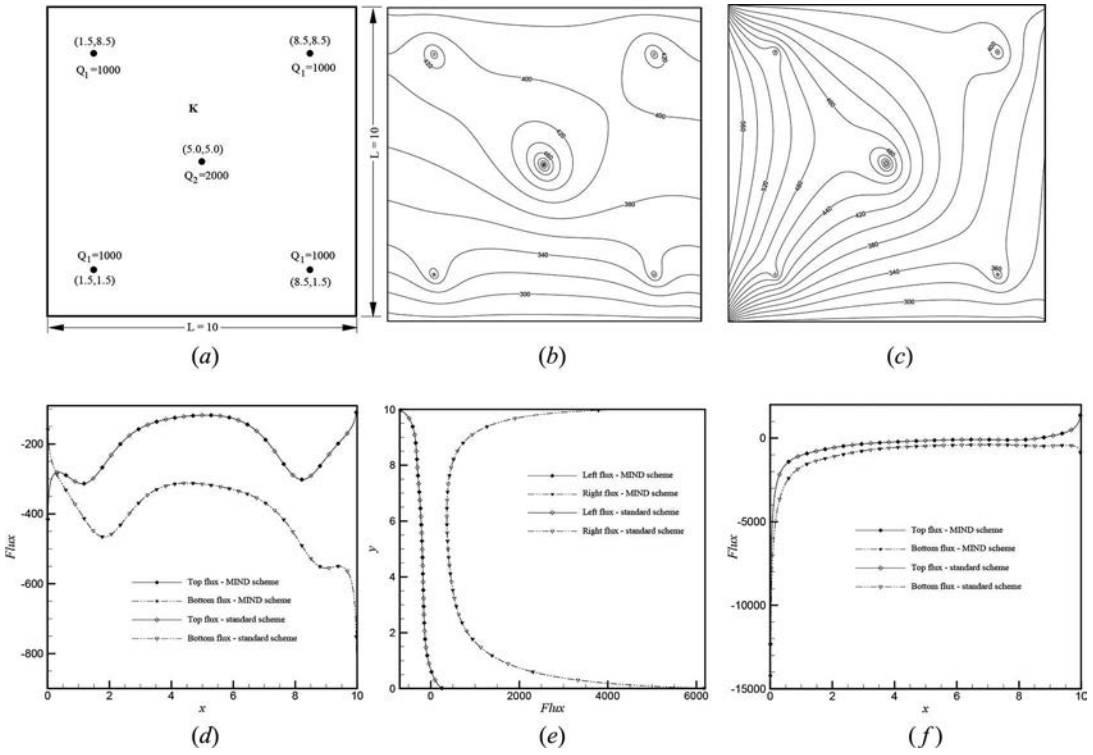

Figure 19. (*a*) Physical situation and boundary conditions for the heterogeneous anisotropic conduction with a point sources problem; ϕ-contours for the case of (*b*) Von Neumann and (*c*) Robin-type boundary condition; (*d*) variation of fluxes along the top and bottom walls for the case of Von Neumann condition with zero flux along the left and right vertical walls of the domain; variation of fluxes along (*e*) the left and right vertical walls and (*f*) the top and bottom walls for the case of Robin-type boundary condition along the left and right vertical walls of the domain.

In Figure 19(*d*), the fluxes along the lower and upper horizontal wall for the von Neumann condition case are displayed. As shown, fluxes obtained with both schemes are on top of each other. The same is also true for the fluxes along the vertical side walls and horizontal bottom and top walls obtained with the Robin condition and presented in Figures 19(*e*) and 19(*f*), respectively. This confirms the correct treatment of the various types of boundary conditions applicable to the diffusion term with the MIND scheme.

Closing remarks

A fully implicit method for the discretization of the diffusion operator was developed that allows for a robust, accurate, and fully implicit treatment resulting in good convergence characteristics for all types of meshes. The method was implemented in the context of a structured and an unstructured cell-centered FVM using quadrilateral and triangular elements, respectively. Isotropic and anisotropic diffusion test problems were solved through the newly developed MIND scheme, and predictions were compared with similar ones generated using the semi-implicit discretization scheme. The results obtained demonstrated the accuracy, higher convergence rate, and boundedness of the MIND scheme. The fully implicit discretization feature of the method is expected to be of high benefit in the discretization of the pressure equation in pressure-based coupled flow solvers, which is a research topic currently under consideration.

Acknowledgment

The support provided by the American University of Beirut and HSLU in the name of Prof. E. Casartelli is gratefully acknowledged.

References

[1] S. V. Patankar, *Numerical Heat Transfer and Fluid Flow*, Hemisphere Publishing, New York, NY, 1980.
[2] C. Hirsch, *Numerical Computation of Internal and External Flows*, vols. 1, 2, John Wiley & Sons Ltd., Chichester, 1984.
[3] J. Ferziger and M. Peric, *Computational Methods for Fluid Dynamics*, 3rd ed., Springer, Berlin, Germany, 2002.
[4] ANSYS Fluent, http://www.ansys.com
[5] Star-CD, http://www.cd-adapco.com/products/star-cd®
[6] Numeca, http://www.numeca.com/en
[7] H. G. Weller, G. Tabor, H. Jasak, C. Fureby, and A. Tensorial, Approach to Computational Continuum Mechanics Using Object-Oriented Techniques, *Comput. Phys.*, vol. 12, no. 6, pp. 620–631, 1998.
[8] F. Palacios, M. Colonno, A. Aranake, A. Campos, S. Copeland, T. Economon, A. Lonkar, T. Lukacyk, T. Taylor, and J. Alonso, Stanford University Unstructured (SU2): An Open-Source Integrated Computational Environment for Multi-Physics Simulation and Design, *51st AIAA Aerospace Sciences Meeting*, Dallas, Texas, January 7–10, 2013.
[9] F. Moukalled, L. Mangani, and M. Darwish, *The Finite Volume Method in Computational Fluid Dynamics: An Advanced Introduction with OpenFOAM® and Matlab®*, Springer, Switzerland, 2015.
[10] M. Darwish and F. Moukalled, A Compact Procedure for Discretization of the Anisotropic Diffusion Operator, *Numer. Heat Transfer Part B Fundam.*, vol. 55, no. 5, pp. 339–360, 2009.
[11] P. A. Jayantha and I. W. Turner, On the Use of Surface Interpolation Techniques in Generalized Finite Volume Strategies for Simulating Transport in Highly Anisotropic Porous Media, *J. Comput. Appl. Math.*, vol. 152, pp. 199–216, 2003.
[12] P. A. Jayantha and I. W. Turner, A Second Order Control-Volume Finite-Element Least-Squares Strategy for Simulating Diffusion in Anisotropic Media, *J. Comput. Appl. Math.*, vol. 23, no. 1, pp. 1–16, 2005.
[13] I. Demirdzic, On the Discretization of the Diffusion Term in Finite-Volume Continuum Mechanics, *Numer. Heat Transfer Part B Fundam.*, vol. 68, no. 1, pp. 1–10, 2015.
[14] I. Demirdzic, A Finite Volume Method for Computation of Fluid Flow in Complex Geometries, Ph.D. Thesis, University of London, 1982.
[15] S. Muzaferija, Adaptive Finite Volume Method for Flow Predictions Using Unstructured Meshes and Multigrid Approach, Ph.D. Thesis, University of London, 1994.

[16] I. Demirdzic and S. Musaferija, Numerical Method for Coupled Fluid Flow, Heat Transfer and Stress Analysis Using Unstructured Moving Meshes with Cells of Arbitrary Topology, *Comput. Methods Appl. Mech. Eng.*, vol. 125, pp. 235–255, 1995.
[17] S. R. Mathur and J. Y. Murthy, A Pressure-Based Method for Unstructured Meshes, *Numer. Heat Transfer B*, vol. 31, pp. 195–215, 1997.
[18] P. J. Zwart, G. D. Raithby, and M. J. Raw, Integrated Space-Time Finite-Volume Mthod for Moving-Boundary Problems, *Numer. Heat Transfer Part B Fundam.*, vol. 34, no. 3, pp. 257–270, 1998.
[19] D. J. Rose, H. Shao, and C. S. Henriquez, Discretization of Anisotropic Convection-Diffusion Equations, Convective M-Matrices and their Iterative Solution, *VLSI Des.*, vol. 10, no. 4, pp. 485–529, 2000.
[20] S. Wang, Solving Convection-Dominated Anisotropic Diffusion Equations by an Exponentially Fitted Finite Volume Method, *Comput. Math. Appl.*, vol. 44, pp. 1249–1265, 2002.
[21] E. Bertolazzi and G. Manzini, A Second-Order Maximum Principle Preserving Finite Volume Method for Steady Convection–Diffusion Problems, *SIAM J. Numer. Anal.*, vol. 43, no. 5, pp. 2172–2199, 2006.
[22] K. Domelevo and P. Omnes, A Finite Volume Method for the Laplace Equation on Almost Arbitrary Two-Dimensional Grids, *ESAIM Math. Modell. Numer. Anal.*, vol. 39, no. 6, pp. 1203–1249, 2005.
[23] E. Eymard, T. Gallouêt, and R. Herbin, A Finite Volume Scheme for Anisotropic Diffusion Problems, *Comptes Rendus Math.*, vol. 339, no. 4, pp. 299–302, 2004.
[24] P. G. Ciarlet, Discrete Maximum Principle for Finite Difference Operators, *Aequationes Math.*, vol. 4, pp. 338–352, 1970.
[25] V. S. Borisov, On Discrete Maximum Principles for Linear Equation Systems and Mono-Tonicity of Difference Schemes, *SIAM J. Matrix Anal. Appl.*, vol. 24, pp. 1110–1135, 2003.
[26] V. S. Borisov and S. Sorek, On the Monotonicity of Difference Schemes for Computational Physics, *SIAM J. Sci. Comput.*, vol. 25, pp. 1557–1584, 2004.
[27] B. P. Leonard, Simple High-Accuracy Resolution Program for Convective Modelling of Discontinuities, *Int. J. Numer. Methods Eng.*, vol. 8, pp. 1291–1318, 1988.
[28] M. Darwish, A New High Resolution Scheme Based on the Normalized Variable Formulation, *Numer. Heat Transfer Part B: Fundam.*, vol. 24, pp. 353–371, 1993.
[29] X. Liu, P. Ming, W. Zhang, L. Fu, and L. Jing, Finite-Volume Methods for Anisotropic Diffusion Problems on Skewed Meshes, *Numer. Heat Transfer Part B: Fundam.*, vol. 68, no. 3, pp. 239–256, 2015.
[30] M. V. Umansky, M. S. Day, and T. D. Rognlien, On Numerical Solution of Strongly Anisotropic Diffusion Equation on Misaligned Grids, *Numer. Heat Transfer Part B: Fundam.*, vol. 47, no. 6, pp. 533–554, 2005.
[31] S. L. Truscott and I. W. Turner, An Investigation of the Accuracy of the Control-Volume Finite-Element Method Base on Triangular Prismatic Elements for Simulating Diffusion in Anisotropic Media, *Numer. Heat Transfer Part B: Fundam.*, vol. 46, no. 3, pp. 243–268, 2004.
[32] I. Aavatsmark, An Introduction to Multipoint Flux Approximations for Quadrilateral Grids, *Comput. Geosci.*, vol. 6, pp. 405–432, 2002.
[33] I. Aavatsmark, G. Eigestad, B. Mallison, and J. Nordbotten, A Compact Multipoint Flux Approximation Method with Improved Robustness, *Numer. Methods Partial Differ. Equations*, vol. 24, no. 5, pp. 1329–1360, 2008.
[34] G. Manzini and M. Putti, Mesh Locking Effects in the Finite Volume Solution of 2-D Anisotropic Diffusion Equations, *J. Comput. Phys.*, vol. 220, pp. 751–771, 2007.
[35] C. Le Potier, Schema Volumes Finis Monotone pour des Operateurs de Diffusion Fortement Anisotropes sur des Maillages de Triangle Non Structures, *Comptes Rendus Math.*, vol. 341, pp. 787–792, 2005.
[36] K. Lipnikov, D. Svyatskiy, M. Shashkov, and Y. Vassilevski, Monotone Finite Volume Schemes for Diffusion Equations on Unstructured Triangular and Shape-Regular Polygonal Meshes, *J. Comput. Phys.*, vol. 227, pp. 492–512, 2007.
[37] K. Lipnikov, D. Svyatskiy, and Y. Vassilevski, Interpolation-Free Monotone Finite Volume Method for Diffusion Equations on Polygonal Meshes, *J. Comput. Phys.*, vol. 228, pp. 703–716, 2009.
[38] K. Nikitin and Y. Vassilevski, A Monotone Nonlinear Finite Volume Method for Advection–Diffusion Equations on Unstructured Polyhedral Meshes in 3D, *Russ. J. Numer. Anal. Math. Modell.*, vol. 25, no. 4, pp. 335–358, 2010.
[39] I. Kapyrin, A Family of Monotone Methods for the Numerical Solution of Three-Dimensional Diffusion Problems on Unstructured Tetrahedral Meshes, *Dokl. Math.*, vol. 76, no. 2, pp. 734–738, 2007.
[40] C. Le Potier, Finite Volume Scheme Satisfying Maximum and Minimum Principles for Anisotropic Diffusion Operators, in R. Eymard and J. M. Herard (eds.), *Finite Volume for Complex Applications*, pp. 103–118, Wiley-ISTE, London, 2008.
[41] K. Lipnikov, D. Svyatskiy, and Y. Vassilevski, Minimal Stencil Finite Volume Scheme with the Discrete Maximum Principle, *Russ. J. Numer. Anal. Math. Modell.*, vol. 27, no. 4, pp. 369–385, 2012.
[42] K. Lipnikov, D. Svyatskiy, and Y. Vassilevski, A Monotone Finite Volume Method for Advection-Diffusion Equations on Unstructured Polygonal Meshes, *J. Comput. Phys.*, vol. 229, pp. 4017–4032, 2010.
[43] C. Le Potier, A Finite Volume Method for the Approximation of Highly Anisotropic Diffusion Operators on Unstructured Meshes, *Finite Volumes for Complex Applications IV*, Marrakech, Marocco, July 4–8, 2005.

[44] M. Darwish and F. Moukalled, Normalized Variable and Space Formulation Methodology for High-Resolution Schemes, *Numer. Heat Transfer Part B: Fundam.*, vol. 26, no. 1, pp. 79–96, 1994.
[45] F. Moukalled and M. Darwish, New Family of Adaptive Very High Resolution Schemes, *Numer. Heat Transfer Part B: Fundam.*, vol. 34, pp. 215–239, 1998.
[46] M. Darwish and F. Moukalled, The χ-Schemes: A New Consistent High-Resolution Formulation Based on the Normalized Variable Methodology, *Comput. Methods Appl. Mech. Eng.*, vol. 192, pp. 1711–1730, 2003.
[47] M. Darwish and F. Moukalled, TVD Schemes for Unstructured Grids, *Int. J. Heat Mass Transfer*, vol. 46, no. 4, pp. 599–611, 2003.
[48] M. Darwish, W. Geahchan, and F. Moukalled, Fully Implicit Coupling for Non-Matching Grids, *International Conference on Numerical Analysis and Applied Mathematics (ICNAAM 2010), AIP Conference Proceedings*, Crete, Greece, 19–25 September, 2010.
[49] M. Darwish, W. Geahchan, and F. Moukalled, A Fully Implicit Method for Coupling Multi-Block Meshes with Non-Matching Interface Grids, *Numer. Heat Transfer Part B: Fundam.*, vol. 71, no. 2, pp. 109–132, 2017.
[50] L. Agelas, R. Eymard, and R. Herbin, *A Nine-Point Finite Volume Scheme for the Simulation of Diffusion in Heterogeneous Media*, Comptes Rendus de l'Academie Des Sciences, Paris, Serie I, Mathematique, Elsevier, Paris, France, vol. 347, pp. 673–676, 2009.
[51] V. Venkatakrishnan, On the Accuracy of Limiters and Convergence to Steady State Solutions, AIAA Paper 93–0880, 1993.
[52] V. Venkatakrishnana, Convergence to Steady State Solutions of the Euler Equations on Unstructured Grids with Limiters, *J. Comput. Phys.*, vol. 118, pp. 120–130, 1995.
[53] Z. J. Zang, A FAS Nested Multi-Grid Viscous Flow Solver for Adaptive Cartesian/Quad Grids, *Int. J. Numer. Methods Fluids*, vol. 33, pp. 657–680, 2000.
[54] M. Keyhani and R. A. Polehn, Finite Difference Modeling of Anisotropic Flows, *ASME J. Heat Transfer*, vol. 117, pp. 458–464, 1995.
[55] A. I. Shestakov, D. S. Kershaw, and G. B. Zimmerman, Test Problems in Radiative Transfer Calculations, *Nuclear Sci. Eng.*, vol. 105, no. 1, pp. 88–104, 1990.
[56] M. Mlacnik, L. Durlofsky, R. Juanes, and H. Tchelepi, Multipoint Flux Approximations for Reservoir Simulation, *12th annual SUPRI-HW Meeting*, Standford University, November 18–19, 2004.